

Ionization Mechanism and Chemical Composition of an Argon DC Discharge with Water Cathode

Dmitriy A. Shutov · Sergey A. Smirnov · Elena Bobkova · Vladimir V. Rybkin

Received: 1 October 2014 / Accepted: 2 November 2014 / Published online: 14 November 2014
© Springer Science+Business Media New York 2014

Abstract This paper reports the results of the experimental study and chemical composition modeling for a DC argon discharge burning above water cathode in the pressure range of 0.1–1 bar and at discharge current of 40 mA. The gas temperature, reduced electric field strength, and emission intensities of some argon lines were obtained. On the base of these data, the modeling chemical composition of plasma was carried out. At modeling, the combined solution of Boltzmann equation for electrons, equations of vibrational kinetics for ground states of N₂, O₂, H₂O and NO molecules, equations of chemical kinetics and plasma conductivity equation was used. The calculations agree well with the measured line intensities. It was shown that discharge burns in diffusion mode, at which the stepwise ionization rate of four lower excited states of argon is equal to the rate of charges diffusion losses.

Keywords DC argon discharge · Water cathode · Modeling · Plasma composition · Ionization mechanism

Introduction

The large number of works published in recent years on studies of non-equilibrium plasma of atmospheric pressure in contact with solutions emphasizes the interest in this field of plasma physics and plasma chemistry [1]. Plasma is a source of various kinds of active species. Some of them (e.g. O, ·OH, HO₂·, ·H radicals and H₂O₂) can be formed in the gas

D. A. Shutov · S. A. Smirnov · V. V. Rybkin (✉)
Department of Microelectronic Devices and Materials, Ivanovo State University of Chemistry and Technology, 153000 IvanovoF. Engels Ave., 7, Russia
e-mail: rybkin@isuct.ru

E. Bobkova
Department of Industrial Ecology, Ivanovo State University of Chemistry and Technology,
153000 IvanovoF. Engels Ave., 7, Russia

phase followed by their penetration into the solution. Other particles react with water molecules at the gas–liquid interface resulting in non-equilibrium water dissociation under the action of ion–electron bombardment and VUV radiation. For understanding the mechanisms of the processes, it is necessary to know the active species concentrations in a gas phase and their change under variations of discharge parameters. Except for ozone concentration, such data are rather limited. Independently on a discharge type, the emission spectra show the radiation bands of excited states of N_2 , OH and NO and lines of atomic H and O at discharge in air or oxygen [2]. However, quantitative data are lacking. There are some studies where the OH radical concentrations in the ground state were measured in a gas phase for the atmospheric pressure DC discharge with aqueous cathode in an ambient air, He, Ar and N_2 by a LIF method [3, 4] and applying the absorption in UV region for Ar/ H_2O [5]. For air, it was discovered that OH concentration was about 10^{15} – 10^{16} cm^{-3} in the current range of 10–30 mA. It is safe to say that measurements of species densities in liquid plasmas are largely an unexplored area. For this reason, modeling becomes an efficient method to study plasma composition.

As for plasmas which are not in a contact with water solutions there are several studies devoted to modeling chemical composition of gas phase containing additions of water vapor.

In study [6], a zero-dimension global model was developed for plasma chemical processes in the helium RF atmospheric pressure discharge with admixture of water molecules. Authors did not use any experimental data on plasma parameters. The input data for the calculation were the electron density and the initial composition of plasma-forming gas. The discharge power and, therefore, the reduced field strength, E/N , were determined from the balance equations of charged particles. Gas temperature was assumed to be 300 K. The rate coefficients for processes of electron impact were determined by means of the Boltzmann equation solution.

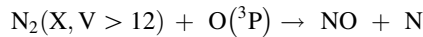
The plasma chemistry processes were simulated in study [7] for an atmospheric pressure RF discharge (13.56 MHz) in helium containing admixtures of O_2 and humid air. The O_2 content was 0.5 % and humid air one was 0.05 %. The air composition included 10^{-2} % of CO_2 , 10^{-3} % of N_2O , 10^{-5} % of NO_2 , and 10^{-6} % of NO. Water content in air was varied in the range of 0–2.3 %. For the simulation, authors used 0-D and 1-D Global models. To calculate the rate constants of electron impact, the Boltzmann equation was used. Both models showed good agreement.

In study [8], a zero-dimension modeling of the chemical composition was carried out for an atmospheric pressure argon plasma jet flowing into humid air. The reaction chemistry set for an argon/humid air mixture was developed, which considers 84 different species and 1,880 reactions. Modeling results agreed satisfactorily with experimental values of ozone concentrations, which were measured in study [9] by adsorption method.

Numerical analysis of the NO and O generation mechanism in the RF atmospheric pressure needle-type plasma jet (Ar + 2 % of air) was carried out in study [10]. For the model verification, authors used the concentrations of NO molecules and O atoms, which were measured experimentally. The calculation results and experimental data agree between each other. Modeling showed that water molecules additions from 1 up to 500 ppm must result in threefold density decrease of O atoms.

In spite of the fact that the models mentioned above are extremely useful for understanding the discharge physics and chemistry, their results depend on discharge type since plasma parameters such as electron densities, electric field strengths, electron energy function distributions, gas temperatures etc. can differ strongly. Thus, for RF atmospheric pressure needle-type plasma jet, the typical values of gas temperatures and electron

densities were ~ 600 K and $\sim 10^{11}$ cm $^{-3}$ [9, 10]. As it will be shown below, for a DC discharge above water surface, the appropriate values are $\sim 1,400$ K and $\sim 10^{13}$ cm $^{-3}$. It can lead to changes in the processes mechanism. For example, in study [10] the reactions of NO formation with participation of vibrationally excited nitrogen molecules in ground electronic state were not taken into account. Though, the result obtained agrees with the experiment. At the same time, in study [11, 12] it was shown that the reaction



is a main way of NO molecules formation for low pressure DC discharge.

As far as we know there is not the detail analysis of processes kinetics proceeding in an argon DC discharge burning in contact with water cathode. Among different types of discharges in contact with water, a DC discharge above liquid is the one having advantage of easy optical access to the plasma. Therefore, the emission intensities can be used for the model verification.

To create a model which allows calculating the plasma properties on the base of external parameters (pressure, initial gas composition, and discharge current) only, it is necessary to know the ionization mechanism that is to reveal the main channels of formation and loss of charges. That balance determines the reduced field strength, which is necessary for the stationary discharge burning. The main aim of the given work is to study this problem for the DC discharge in argon burning above water cathode on the base of some experimental results and modeling of plasma composition.

Experimental

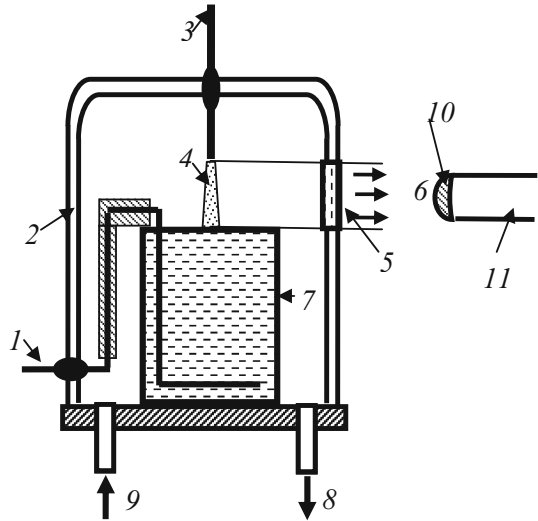
Figure 1 shows a schematic diagram of the experimental set-up. The glass cell with distilled water was placed into a 5 l glass bell-jar. The water volume was 80 ml. Argon of the ultra high purity grade was used as a plasma-forming gas. The gas flow rate was 3 cm 3 s $^{-1}$. The anode was made from mechanically sharpened stainless steel wire (radius of curvature is ~ 100 μm). A DC power supply with a 30 k Ω ballast resistor was used to excite the discharge. A high voltage (up to 4 kV) was applied between the aqueous cathode and anode, which was placed at the position 1–10 mm (typically 4 mm) above the liquid surface. The distance between the anode and the liquid surface was adjustable. The discharge current was 40 mA. The Ar pressure was varied from 0.1 to 1 (± 0.01) bar. The emission spectra were recorded within the wavelength range of 200–950 nm using the AvaSpec-2048FT-2 monochromator (grating of 600 line/mm) with spectrum digital registration. The light entered the monochromator entrance slit through a quartz optical fiber. The light guide-monochromator system was calibrated by the monochromator manufacturer on a radiation power.

The average on the discharge volume the lines intensity, \bar{I} , was determined as follows. The quanta amount, $d\Phi$, emitted with the discharge volume dV into solid angle $\Omega(r, \phi, z)$ per unit of time is.

$$d\Phi = \frac{I}{4 \times \pi} \times \Omega \times dV = \frac{I(r, \phi, z)}{4 \times \pi} \times \Omega \times r dr d\phi dz,$$

where I —line intensity (quantum/(s \times cm 3)); r, ϕ and z —cylindrical coordinates of emitting discharge point. Since the discharge radius ($R_D \approx 1.5$ mm) and discharge length ($L_D = 4$ mm) are much less than the distance between the light guide entrance lens and the

Fig. 1 Schematic diagram of the experimental set-up. 1—cathode, 2—glass bell-jar, 3—anode, 4—discharge, 5—quartz window, 6—radiation output to entrance lens of light guide, 7—glass cell with distilled water, 8, 9—gas outlet and inlet, 10—entrance lens of light fiber, 11—light fiber



discharge ($L = 75$ mm), the Ω value is approximately the same for every discharge point and equals to

$$\Omega = \frac{\pi \times R_L^2}{L^2},$$

where R_L —radius of entrance lens (2.5 mm).

Therefore, the total amount of quanta, Φ , which is registered by monochromator per second, can be written as

$$\Phi = \frac{R_L^2}{4 \times L^2} \times \int_0^{R_D} \int_0^{2\pi} \int_0^{L_D} I \times r dr d\phi dz = \frac{R_L^2}{4 \times L^2} \times \bar{I} \times V_D,$$

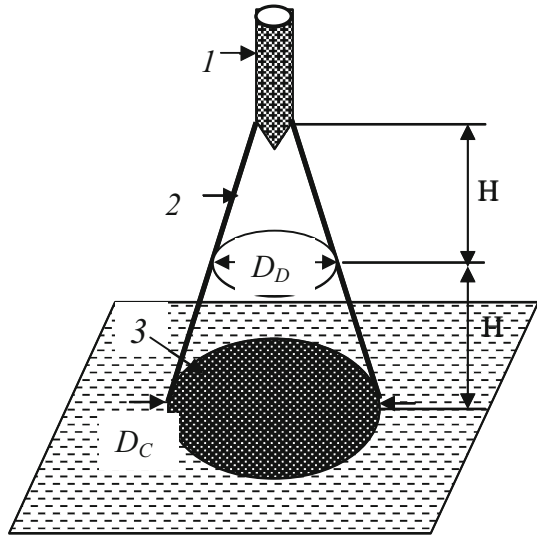
where \bar{I} —average on the discharge volume intensity, V_D —discharge volume.

Actually, the emission from cathode and anode discharge parts was cut off by the size of the quartz window (Fig. 1).

The diagrammatic representation of the discharge is shown in Fig. 2. The typical shape is a cone with clearly delineated cathode spot. The size of this spot was used as a base one for the determination of the discharge geometric parameters using a digital camera. Of course, there is some uncertainty in geometric parameters since the slight diffuse glow is observed outside the borders of the cone.

For the determination of the electric field strength, E , in a positive column, the discharge voltage drop between anode and cathode was measured as a function of anode-surface water distance. The digital voltmeter Fluke 289[®] (USA) was used for this purpose. Voltage drop on water was measured at a contact of anode with water surface. Then, this value was subtracted from the total voltage measured. The linear part of volt-distance dependence was treated with a least-squares method to obtain the electric field strength in a plasma column.

Fig. 2 The diagrammatic representation of discharge. 1— anode, 2—positive column, 3— cathode spot onto the solution surface, $D_D = 2R$ —the effective discharge diameter (radius), D_C —the diameter of cathode spot



To determine the gas temperature, the small addition (1 %) of molecular nitrogen was introduced into the main gas. The rotational temperature was determined by means of treatment of non-resolved rotational structure of the band appropriated to transition $C^3-\Pi_u \rightarrow B^3\Pi_g$ (0–2) as it was described elsewhere [2]. In the present case, the rotational temperature is equal to the translational one. The possibility of applying this method was additionally checked. The MDR-23 spectrometer was utilized. Its grating of 1,200 line/mm allows us to obtain the resolved structure of R_1 -branch (for $J' > 15$) and unresolved one depending on the split sizes. The temperatures obtained were the same within the range of ± 40 K.

The reproducibility errors for all measured values were calculated on the base of five and more measurements using the confidence probability of 0.95. The total errors are shown on appropriate figures as the bars.

All measurements were carried out after reaching the stationary conditions. It was controlled by temporal behavior of line intensities (actually, in 15 min. of discharge burning). The discharge action was accompanied by the reduction of solution pH from 6.2 (initial value) up to 5.5. The last value was reached after ~ 10 min of the discharge action and did not change during ~ 20 min. The time of the pH stabilization approximately coincided with reaching the stable values of the line intensities.

Description of the Model and Calculations

The model included the Boltzmann equation for electrons, equations of vibration kinetics, chemical kinetics equations, and equation of plasma conductivity. The last one was used for determination of electron density on the base of the measured current density.

The electron energy distribution function (EEDF) was obtained from the solution of the homogeneous Boltzmann equation using the two-term expansion in spherical harmonics. Collision integrals concerning charge particle formation were written as for usual inelastic processes. This is possible because the electron energy losses in these processes are

negligible (<0.01 %) compared to the losses for other inelastic processes. It means that the Boltzmann equation can be independently solved using charge balance equations. Collision integrals include the collisions of electrons with Ar, N₂, O₂, H₂O, NO molecules in electronic ground state and with O(³P) atoms. The collisions of the second kind with vibrationally excited molecules and with lower excited states of Ar (¹P₁, ³P₀, ³P₁, ³P₂), O₂(a¹Δ_g) and of O(3s³S, 3s⁵S) were taken into consideration as well. The cross-section sets for Ar, N₂, O₂, H₂O, NO, H₂ molecules and O(³P) atoms were taken from studies [13–19], respectively. It is necessary to point out that NO, H₂, O₂ molecules and O(³P) did not practically influence on the EEDF calculation due to low mole fraction (much <1 %). Since the excitation energy of argon states starts from 11.55 eV and argon shows the Ramsauer effect for the momentum transfer cross-section, it was necessary to take into account the N₂ present in gas mixture in spite of its low concentration (1 %). Unlike argon N₂ molecules have the large cross-sections for electron impact with excitation of vibration and electronic states in this region. The e–e collisions were taken into consideration as well. Mathematical details of the solution were described by us elsewhere [20, 21].

The cross-sections, σ_{ik}, for the stepwise processes of 4p(³S₁, ³D₃, ³D₂, ³D₁, ¹D₂, ³P₀, ¹P₁, ³P₂, ³P₁ ¹S₀) states excitation from 4 s(¹P₁, ³P₀, ³P₁, ³P₂) states by electron impact were calculated by Drawin’s semi-empirical expression [22]:

$$\sigma_{ik} = 4\pi a_0^2 \left(\frac{Ry}{\varepsilon_i}\right)^2 f_{ik} \left\{ \frac{u}{(u+1)^2} \ln \left[1.25(u+1) + \frac{0.1}{u+1} \right] \right\},$$

where a₀ = 0.5292 × 10⁻⁸ cm, Ry = 13.606 eV, ε_i = E_i - E_k—threshold energy, f_{ik}—oscillator strength for i → k transition, u = (ε - ε_i)/ε_i—dimensionless electron energy, ε—electron energy.

The oscillator strengths were calculated from radiation transition probabilities taken from [23].

The cross sections of stepwise ionization by electron impact from ¹P₁, ³P₀, ³P₁, ³P₂ states were calculated by Gryzinsky’s formula [22]

$$\sigma_n = 4\pi a_0^2 \zeta_n \left(\frac{Ry}{I_n}\right)^2 \frac{1}{x} \left(\frac{x-1}{x+1}\right)^{3/2} \left\{ 1 + \frac{2}{3} \left(1 - \frac{1}{2x}\right) \ln \left[2.7 + (x-1)^{1/2} \right] \right\}$$

where I_n = I_{Ar} - E_n, I_{Ar} = 15.755 eV—Ar ground state ionization energy, E_n—energy of n-level, x = ε/I_n, E—electron energy, ζ_n—number of equivalent electrons on external shell of n-state.

The reabsorption of radiation was taken into consideration as well as follows. The effective probability for transition between k and i energy levels, A_{ki}^{eff}, can be written as A_{ki}^{eff} = A_{ki} · g, where A_{ki} is the radiative transition probability, g is escaping factor of radiation. This factor is equal to

$$g = g_D \exp\left(-\frac{g_{LD}^2}{g_L^2}\right) + g_L \cdot \frac{2}{\sqrt{\pi}} \int_0^{\frac{g_{LD}}{g_L}} \exp(-X^2) dX,$$

where g_D is escaping factor for Doppler profile of radiation line and absorption line, g_D is escaping factor for Lorentz profile of radiation line and absorption line, g_{LD} is escaping factor for Lorentz profile of radiation line and the Doppler profile of absorption line. The escaping factors are determined as

$$\begin{aligned}
 (g_D) &= \frac{2}{\sqrt{\pi}} \int_0^\infty e^{-X^2} \cdot \exp\left[-(K_0^D \cdot R) \cdot e^{-X^2}\right] dX \\
 (g_L) &= \frac{2}{\pi} \int_0^\infty \exp\left[-\frac{(K_0^L \cdot R)}{1 + X^2}\right] \frac{dX}{(1 + X^2)} \\
 (g_{LD}) &= \frac{2}{\pi} \int_0^\infty \frac{dX}{X^2 + 1} \cdot \exp\left[-(K_0^D \cdot R) \cdot \exp\left[-\left(\frac{\gamma/2}{\Delta\omega_D}\right)^2 \cdot X^2\right]\right]
 \end{aligned}$$

In these expressions the K_0^D and K_0^L are absorption coefficients in a line centre for appropriate profile, R is length of absorption zone (radius of positive column).

The absorption coefficients are determined as follows:

$$K_0^D = \frac{g_k}{g_i} \frac{\lambda_{ki}^2}{4\sqrt{\pi} \Delta\omega_D} A_{ki} \cdot N_i, \quad K_0^L = \frac{g_k}{g_i} \frac{\lambda_{ki}^2}{2\pi} A_{ki} N_i \cdot (\gamma)^{-1},$$

where g_k and g_i are statistical weights of upper and lower levels, λ_{ki} is wave length, $\Delta\omega_D$ is Doppler half-width of line, N_i is particle concentration on lower level, γ is doubled total frequency of upper level quenching for all collision processes.

The population of vibrational levels of N_2 , O_2 , H_2O , NO molecules in ground state was determined by means of solving the equations system of quasi-stationary kinetics. This system takes into consideration the single-quantum V–V, and V–T exchange including the collisions with Ar atoms, e–V pumping and some other ones. The detailed processes list and data on the rate constants determination is given in study [24].

The equations of chemical kinetics included the set of reactions which are listed in Table 1.

The two-body reactions were taken from the reaction sets proposed in studies [11, 12, 20, 25] for modeling reaction mechanisms in a plasma of oxygen, air and mixtures of argon-oxygen. These sets describe the experimental data quite well for DC discharges. Three-body reactions were chosen according to studies [24, 26, 27]. Of course, there are the studies containing much more reactions. Specifically, study [10] devoted to kinetic modeling for an atmospheric pressure argon plasma jet in a humid air considers about 1,500 processes. But about two thirds of them are the ion–molecule reactions and reactions of charge recombination. The rates of these reactions are limited by the rates of primary processes of ionization. Under our experimental conditions ($E/N \sim 20$ Td), the ionization rates are less than the rates of excitation and dissociation by more than one order of magnitude. Thus, at $E/N = 20$ Td the total ionization rate of Ar atoms (including stepwise ionization) is $6 \times 10^{16} \text{ cm}^{-3} \text{ s}^{-1}$ (see Fig. 12), whereas the total formation rate of Ar ($^1P_1, ^3P_0, ^3P_1, ^3P_2$) states is $1.4 \times 10^{18} \text{ cm}^{-3} \text{ s}^{-1}$. That is why the ion-molecular reactions did not practically act on the kinetics of neutral species. Of course, if the task is to estimate the plasma ions composition, the appropriate reactions have to be added. But it was not the aim of the given study.

The modeling was carried out as follows:

1. The Boltzmann equation was solved for a given E/N , gas temperature, discharge current density, initial composition of mixture (ground state of Ar and 1 % of N_2). Rate coefficients for electron impact as well as electron density were determined.

Table 1 Processes and corresponding rate constants

| No | Process | Rate constants (s^{-1}) ($cm^3 s^{-1}$) ($cm^6 s^{-1}$) | Ref |
|----|---------------------------------------------------------------|--------------------------------------------------------------------|------|
| 1 | $O_2(X) + e \rightarrow O_2(a^1\Delta) + e$ | $f(E/N)$ | |
| 2 | $O_2(a^1\Delta) + e \rightarrow O_2(X) + e$ | $f(E/N)$ | |
| 3 | $O_2(X) + e \rightarrow O_2(b^1\Sigma) + e$ | $f(E/N)$ | |
| 4 | $O_2(X) + e \rightarrow O_2(A^3\Sigma) + e$ | $f(E/N)$ | |
| 5 | $O_2(b^1\Sigma) + e \rightarrow O_2(a^1\Delta) + e$ | $f(E/N)$ | |
| 6 | $O_2(b^1\Sigma) + e \rightarrow O_2(X) + e$ | $f(E/N)$ | |
| 7 | $O_2(X) + O_2(X) + e \rightarrow O_2^- + O_2(X)$ | 2×10^{-30} | [35] |
| 8 | $O_2(a^1\Delta) + e \rightarrow O^- + O(^3P)$ | $f(E/N)$ | |
| 9 | $O_2(a^1\Delta) + e \rightarrow O_2(b^1\Sigma) + e$ | $f(E/N)$ | |
| 10 | $O(^1D) + e \rightarrow O(^3P) + e$ | $f(E/N)$ | |
| 11 | $O(^1S) + e \rightarrow O(^3P) + e$ | $f(E/N)$ | |
| 12 | $O_2(X) + e \rightarrow O(^3P) + O(^3P) + e$ | $f(E/N)$ | |
| 13 | $O_2(X) + e \rightarrow O(^3P) + O(^1D) + e$ | $f(E/N)$ | |
| 14 | $O(^3P) + e \rightarrow O(^1D) + e$ | $f(E/N)$ | |
| 15 | $O(^3P) + e \rightarrow O(^1S) + e$ | $f(E/N)$ | |
| 16 | $O_3 + e \rightarrow O(^3P) + O_2(X) + e$ | $10(K_{12} + K_{13})$ | [36] |
| 17 | $O_2(X) + e \rightarrow O^- + O(^3P)$ | $f(E/N)$ | |
| 18 | $O(^1D) + O(^3P) \rightarrow O(^3P) + O(^3P)$ | 1.5×10^{-11} | [36] |
| 19 | $O_3 + e \rightarrow O(^3P) + O_2^-$ | 1×10^{-9} | [36] |
| 20 | $O_2^- + O_2(a^1\Delta) \rightarrow 2O_2(X) + e$ | 2×10^{-10} | [37] |
| 21 | $O_2^- + O_2(b^1\Sigma) \rightarrow 2O_2(X) + e$ | 3.6×10^{-10} | [38] |
| 22 | $O_2(A^3\Sigma) + O(^3P) \rightarrow O_2(X) + O(^1S)$ | 1.4×10^{-11} | [39] |
| 23 | $O^- + O_2(a^1\Delta) \rightarrow O_3 + e$ | 3×10^{-10} | [37] |
| 24 | $O^- + O_2(b^1\Sigma) \rightarrow O(^3P) + O_2(X) + e$ | 6.9×10^{-10} | [36] |
| 25 | $O(^3P) + O_3 \rightarrow O_2(a^1\Delta) + O_2(X)$ | $2 \times 10^{-11} \exp(-2280/T)$ | [36] |
| 26 | $O_2^- + O(^3P) \rightarrow O_3 + e$ | 1.5×10^{-10} | [37] |
| 27 | $O^- + O(^3P) \rightarrow O_2(X) + e$ | 5×10^{-10} | [40] |
| 28 | $O_2(b^1\Sigma) + O_3 \rightarrow O(^3P) + 2O_2(X)$ | 1.8×10^{-11} | [41] |
| 29 | $O_2(b^1\Sigma) + O_2(X) \rightarrow O_2(a^1\Delta) + O_2(X)$ | $4.3 \times 10^{-22} T^{2.4} \exp(-241/T)$ | [42] |
| 30 | $O_2(b^1\Sigma) + O(^3P) \rightarrow O_2(a^1\Delta) + O(^3P)$ | 8×10^{-14} | [41] |
| 31 | $O_2(b^1\Sigma) + O(^3P) \rightarrow O_2(X) + O(^1D)$ | $3.39 \times 10^{-11} (300/T)^{0.1} \exp(-4201/T)$ | [43] |
| 32 | $O_2(A^3\Sigma) + O_2(X) \rightarrow 2O_2(b^1\Sigma)$ | 2.93×10^{-13} | [39] |
| 33 | $O_2(A^3\Sigma) + O(^3P) \rightarrow O_2(b^1\Sigma) + O(^1D)$ | 9×10^{-12} | [39] |
| 34 | $O(^1D) + O_2(X) \rightarrow O(^3P) + O_2(b^1\Sigma)$ | $2.56 \times 10^{-11} \exp(67/T)$ | [44] |
| 35 | $O(^1D) + O_2(X) \rightarrow O(^3P) + O_2(X)$ | $6.4 \times 10^{-12} \exp(67/T)$ | [45] |
| 36 | $O(^1S) + O_3 \rightarrow O(^1D) + O(^3P) + O_2(X)$ | 2.9×10^{-10} | [45] |
| 37 | $O(^1S) + O_3 \rightarrow O_2(X) + O_2(X)$ | 2.9×10^{-10} | [45] |
| 38 | $O(^1S) + O_2(a^1\Delta) \rightarrow O(^3P) + O_2(A^3\Sigma)$ | 1.3×10^{-10} | [46] |
| 39 | $O(^1S) + O(^3P) \rightarrow O(^1D) + O(^3P)$ | $5 \times 10^{-11} \exp(-301/T)$ | [47] |
| 40 | $O_2(a^1\Delta) + O_2(X) \rightarrow 2O_2(X)$ | $2.2 \times 10^{-18} (T/300)^{0.8}$ | [42] |
| 41 | $O(^1S) + O_2(X) \rightarrow O(^3P) + O_2(A^3\Sigma)$ | $3.17 \times 10^{-12} \exp(-850/T)$ | [48] |
| 42 | $O(^1S) + O_2(X) \rightarrow O(^1D) + O_2(X)$ | $1.43 \times 10^{-12} \exp(-850/T)$ | [48] |
| 43 | $N_2(X) + e \rightarrow N_2(A) + e$ | $f(E/N)$ | |

Table 1 continued

| No | Process | Rate constants (s^{-1}) ($cm^3 s^{-1}$) ($cm^6 s^{-1}$) | Ref |
|----|--------------------------------------------------------|--------------------------------------------------------------------|------|
| 44 | $N_2(X) + e \rightarrow N_2(B) + e$ | $f(E/N)$ | |
| 45 | $N_2(X) + e \rightarrow N_2(a) + e$ | $f(E/N)$ | |
| 46 | $N_2(X) + e \rightarrow N_2(C) + e$ | $f(E/N)$ | |
| 47 | $N_2(X) + e \rightarrow 2 N(^4S) + e$ | $f(E/N)$ | |
| 48 | $N(^4S) + e \rightarrow N(^2D) + e$ | $f(E/N)$ | |
| 49 | $N(^4S) + e \rightarrow N(^2P) + e$ | $f(E/N)$ | |
| 50 | $O(^3P) + N(^2P) \rightarrow NO^+ + e$ | 1×10^{-12} | [26] |
| 51 | $O_2^- + N_2(A) \rightarrow O_2(X) + N_2(X) + e$ | 2.1×10^{-9} | [49] |
| 52 | $O^- + N_2(A) \rightarrow O(^3P) + N_2(X) + e$ | 2.2×10^{-9} | [49] |
| 53 | $O_2^- + N(^4S) \rightarrow NO_2 + e$ | 5×10^{-10} | [50] |
| 54 | $O^- + N(^4S) \rightarrow NO + e$ | 2.6×10^{-10} | [51] |
| 55 | $O^- + NO \rightarrow NO_2 + e$ | 2.6×10^{-10} | [51] |
| 56 | $N(^4S) + NO \rightarrow N_2(X, V = 11) + O(^3P)$ | $1.05 \times 10^{-12} \times (T)^{1/2}$ | [52] |
| 57 | $NO + O_3 \rightarrow O_2(X) + NO_2$ | $4.3 \times 10^{-12} \times \exp(-1560/T)$ | [52] |
| 58 | $N_2(A) + O_2(X) \rightarrow N_2(X) + 2O(^3P)$ | 2.54×10^{-12} | [53] |
| 59 | $N_2(A) + O(^3P) \rightarrow NO + N(^2D)$ | 2×10^{-11} | [54] |
| 60 | $N_2(A) + N_2(A) \rightarrow N_2(C) + N_2(X)$ | 2×10^{-12} | [55] |
| 61 | $N_2(A) + O_2(X) \rightarrow N_2(X) + O_2(a)$ | 6×10^{-12} | [53] |
| 62 | $N_2(A) + N(^4S) \rightarrow N_2(X) + N(^2P)$ | 5×10^{-11} | [56] |
| 63 | $N_2(A) + O(^3P) \rightarrow N_2(X) + O(^1S)$ | 2.1×10^{-11} | [57] |
| 64 | $N_2(A) + NO \rightarrow N_2(X) + NO$ | 1.1×10^{-10} | [58] |
| 65 | $N_2(B) + N_2(X) \rightarrow N_2(A) + N_2$ | 5×10^{-11} | [56] |
| 66 | $N_2(B) \rightarrow N_2(A) + hv$ | 1.5×10^5 | [59] |
| 67 | $N_2(B) + NO \rightarrow N_2(A) + NO$ | 2.4×10^{-10} | [58] |
| 68 | $N_2(B) + O_2(X) \rightarrow N_2 + 2O(^3P)$ | 3×10^{-10} | [56] |
| 69 | $N_2(a) + N_2(X) \rightarrow N_2(B) + N_2(X)$ | 2×10^{-13} | [60] |
| 70 | $N_2(a) + O_2(X) \rightarrow N_2(X) + O(^3P) + O(^3P)$ | 2.8×10^{-11} | [60] |
| 71 | $N_2(a) + NO \rightarrow N_2(X) + N(^4S) + O(^3P)$ | 3.6×10^{-10} | [60] |
| 72 | $N_2(C) \rightarrow N_2(B) + hv$ | 3×10^7 | [59] |
| 73 | $N_2(C) + O_2(X) \rightarrow N_2(X) + O(^3P) + O(^1S)$ | 3×10^{-10} | [56] |
| 74 | $O_2(a) + NO \rightarrow O_2(X) + NO$ | 2.5×10^{-11} | [61] |
| 75 | $O_2(b) + N_2(X) \rightarrow O_2(a) + N_2(X)$ | $4.9 \times 10^{-15} \times \exp(-253/T)$ | [62] |
| 76 | $O_2(b) + NO \rightarrow O_2(a) + NO$ | 4×10^{-14} | [63] |
| 77 | $O_2(A) + N_2(X) \rightarrow O_2(b) + N_2(X)$ | 3×10^{-13} | [64] |
| 78 | $N(^2D) + O_2(X) \rightarrow NO + O(^3P)$ | $1.5 \times 10^{-12} \times (T/300)^{1/2}$ | [26] |
| 79 | $N(^2D) + O_2(X) \rightarrow NO + O(^1D)$ | $6 \times 10^{-12} \times (T/300)^{1/2}$ | [26] |
| 80 | $N(^2D) + NO \rightarrow N_2(X) + O(^3P)$ | 6×10^{-11} | [45] |
| 81 | $N(^2P) + O_2(X) \rightarrow NO + O(^3P)$ | 2.6×10^{-12} | [65] |
| 82 | $N(^2P) + NO \rightarrow N_2(A) + O(^3P)$ | 3.4×10^{-11} | [66] |
| 83 | $O(^1D) + N_2(X) \rightarrow O(^3P) + N_2(X)$ | $1.8 \times 10^{-11} \times \exp(107/T)$ | [67] |
| 84 | $O(^1D) + NO \rightarrow N(^4S) + O_2(X)$ | 1.7×10^{-10} | [45] |
| 85 | $O(^1S) + NO \rightarrow O(^3P) + NO$ | 1.8×10^{-10} | [45] |
| 86 | $O(^1S) + NO \rightarrow O(^1D) + NO$ | 3.2×10^{-10} | [45] |

Table 1 continued

| No | Process | Rate constants (s^{-1}) ($cm^3 s^{-1}$) ($cm^6 s^{-1}$) | Ref |
|-----|-----------------------------------------------------------|--------------------------------------------------------------------|-------------------|
| 87 | $NO + e \rightarrow N(^4S) + O(^3P) + e$ | $f(E/N)$ | |
| 88 | $O(^3P) + NO + M \rightarrow NO_2 + M$ | $f(T, M)$ | [26] |
| 89 | $O(^3P) + N(^4S) + M \rightarrow NO + M$ | $1.36 \times 10^{-31} T^{-0.5}$ | [26] |
| 90 | $O(^3P) + NO_2 + M \rightarrow NO_3 + M$ | $f(T, M)$ | [26] |
| 91 | $O(^3P) + N_2(X, V) \rightarrow NO + N(^4S)$ | * | [32, 68] |
| 92 | $O_2(b^1\Sigma) \rightarrow O_2(X) + hv$ | 0.085 | [59] |
| 93 | $N_2(C) + N_2(X) \rightarrow N_2(X) + N_2(X)$ | 5×10^{-11} | [56] |
| 94 | $Ar(4p^3D_3) + Ar \rightarrow Ar + Ar$ | $2.2 \times 10^{-10} \times (T/300)^{0.5}$ | [55] ¹ |
| 95 | $Ar(4p^3D_3) + O_2(X) \rightarrow Ar + O_2(X)$ | $2.2 \times 10^{-10} \times (T/300)^{0.5}$ | [69] |
| 96 | $Ar + e \rightarrow Ar(4s^3P_2) + e$ | $f(E/N)$ | |
| 97 | $Ar(4p^3P_1) \rightarrow hv + Ar(4s^3P_2)$ | 7.2×10^6 | [59] |
| 98 | $Ar(4p^3P_2) \rightarrow hv + Ar(4s^3P_2)$ | 4.4×10^6 | [59] |
| 99 | $Ar(4p^1P_1) \rightarrow hv + Ar(4s^3P_2)$ | 0.7×10^6 | [59] |
| 100 | $Ar(4p^1D_2) \rightarrow hv + Ar(4s^3P_2)$ | 27.4×10^6 | [59] |
| 101 | $Ar(4p^3D_1) \rightarrow hv + Ar(4s^3P_2)$ | 5.4×10^6 | [59] |
| 102 | $Ar(4p^3D_2) \rightarrow hv + Ar(4s^3P_2)$ | 9.5×10^6 | [59] |
| 103 | $Ar(4p^3D_3) \rightarrow hv + Ar(4s^3P_2)$ | 35×10^6 | [59] |
| 104 | $Ar(4p^3S_1) \rightarrow hv + Ar(4s^3P_2)$ | 18×10^6 | [59] |
| 105 | $Ar(4s^1P_1) + e \rightarrow Ar(3s^3P_2) + e$ | 3.1×10^{-7} | [70] |
| 106 | $Ar(4s^3P_0) + e \rightarrow Ar(4s^3P_2) + e$ | 3.1×10^{-7} | [70] |
| 107 | $Ar(4s^3P_1) + e \rightarrow Ar(4s^3P_2) + e$ | 3.1×10^{-7} | [70] |
| 108 | $Ar(4s^3P_2) + e \rightarrow Ar(4p^3P_1) + e$ | $f(E/N)$ | |
| 109 | $Ar(4s^3P_2) + e \rightarrow Ar(4p^3P_2) + e$ | $f(E/N)$ | |
| 110 | $Ar(4s^3P_2) + e \rightarrow Ar(4p^1P_1) + e$ | $f(E/N)$ | |
| 111 | $Ar(4s^3P_2) + e \rightarrow Ar(4p^1D_2) + e$ | $f(E/N)$ | |
| 112 | $Ar(4s^3P_2^M) + e \rightarrow Ar(4p^3D_1) + e$ | $f(E/N)$ | |
| 113 | $Ar(4s^3P_2) + e \rightarrow Ar(4p^3D_2) + e$ | $f(E/N)$ | |
| 114 | $Ar(4s^3P_2) + e \rightarrow Ar(4p^3D_3) + e$ | $f(E/N)$ | |
| 115 | $Ar(4s^3P_2) + e \rightarrow Ar(4p^3S_1) + e$ | $f(E/N)$ | |
| 116 | $Ar(4s^3P_2) + e \rightarrow Ar(4s^1P_1) + e$ | 2.35×10^{-7} | [70] |
| 117 | $Ar(4s^3P_2) + e \rightarrow Ar(4s^3P_0) + e$ | 2.35×10^{-7} | [70] |
| 118 | $Ar(4s^3P_2) + e \rightarrow Ar(4s^3P_1) + e$ | 2.35×10^{-7} | [70] |
| 119 | $Ar(4s^3P_2) + e \rightarrow Ar^+ + e$ | $f(E/N)$ | |
| 120 | $Ar(4s^3P_2) + Ar(4s^3P_2) \rightarrow Ar^+ + e$ | 1.2×10^{-9} | [70] |
| 121 | $Ar(4s^3P_2) + Ar(4s^3P_0) \rightarrow Ar^+ + e$ | 1.2×10^{-9} | [70] |
| 122 | $Ar(4s^3P_2) + Ar(4s^3P_1) \rightarrow Ar^+ + e$ | 2.1×10^{-9} | [70] |
| 123 | $Ar(4s^3P_2) + Ar(4s^1P_1) \rightarrow Ar^+ + e$ | 2.1×10^{-9} | [70] |
| 124 | $Ar(4s^3P_2) + 2Ar \rightarrow Ar_2^+ + Ar$ | 11×10^{-32} | [70] |
| 125 | $Ar(4s^3P_2) + Ar \rightarrow Ar + Ar$ | 1.1×10^{-15} | [71] |
| 126 | $Ar(4s^3P_2) + O(^3P) \rightarrow O(3p^3P) + Ar$ | $1.38 \times 10^{-11} \times (T)^{1/2}$ | [72] |
| 127 | $Ar(4s^3P_2) + O_2 \rightarrow Ar(^1S) + O(^1D) + O(^1S)$ | 1.7×10^{-10} | [71] |
| 128 | $Ar + e \rightarrow Ar(4s^3P_1) + e$ | $f(E/N)$ | |
| 129 | $Ar(4p^1S_0) \rightarrow hv + Ar(4s^3P_1)$ | 0.24×10^6 | [59] |

Table 1 continued

| No | Process | Rate constants (s ⁻¹) (cm ³ s ⁻¹) (cm ⁶ s ⁻¹) | Ref |
|-----|-----------------------------------------------------------------------------------------------------------------------------|------------------------------------------------------------------------------------------------------------|------|
| 130 | Ar(4p ³ P ₁) → hv + Ar(4s ³ P ₁) | 1.9 × 10 ⁶ | [59] |
| 131 | Ar(4p ³ P ₂) → hv + Ar(4s ³ P ₁) | 8.9 × 10 ⁶ | [59] |
| 132 | Ar(4p ¹ P ₁) → hv + Ar(³ P ₁) | 0.02 × 10 ⁶ | [59] |
| 133 | Ar(4p ³ P ₀) → hv + Ar(4s ³ P ₁) | 44 × 10 ⁶ | [59] |
| 134 | Ar(4p ¹ D ₂) → hv + Ar(4s ³ P ₁) | 4.6 × 10 ⁶ | [59] |
| 135 | Ar(³ D ₁) → hv + Ar(4s ³ P ₁) | 26 × 10 ⁶ | [59] |
| 136 | Ar(4p ³ D ₂) → hv + Ar(4s ³ P ₁) | 21 × 10 ⁶ | [59] |
| 137 | Ar(4p ³ S ₁) → hv + Ar(4s ³ P ₁) | 5.3 × 10 ⁶ | [59] |
| 138 | Ar(4s ¹ P ₁) + e → Ar(4s ³ P ₁) + e | 3.1 × 10 ⁻⁷ | [70] |
| 139 | Ar(4s ³ P ₀) + e → Ar(4s ³ P ₁) + e | 3.1 × 10 ⁻⁷ | [70] |
| 140 | Ar(4s ³ P ₁) + e → Ar(¹ S ₀) + e | <i>f</i> (<i>E</i> / <i>N</i>) | |
| 141 | Ar(4s ³ P ₁) + e → Ar(4p ³ P ₁) + e | <i>f</i> (<i>E</i> / <i>N</i>) | |
| 142 | Ar(4s ³ P ₁) + e → Ar(4p ³ P ₂) + e | <i>f</i> (<i>E</i> / <i>N</i>) | |
| 143 | Ar(4s ³ P ₁) + e → Ar(4p ¹ P ₁) + e | <i>f</i> (<i>E</i> / <i>N</i>) | |
| 144 | Ar(4s ³ P ₁) + e → Ar(4p ³ P ₀) + e | <i>f</i> (<i>E</i> / <i>N</i>) | |
| 145 | Ar(4s ³ P ₁) + e → Ar(4p ¹ D ₂) + e | <i>f</i> (<i>E</i> / <i>N</i>) | |
| 146 | Ar(4s ³ P ₁) + e → Ar(4p ³ D ₁) + e | <i>f</i> (<i>E</i> / <i>N</i>) | |
| 147 | Ar(4s ³ P ₁) + e → Ar(4p ³ D ₂) + e | <i>f</i> (<i>E</i> / <i>N</i>) | |
| 148 | Ar(4s ³ P ₁) + e → Ar(4p ³ S ₁) + e | <i>f</i> (<i>E</i> / <i>N</i>) | |
| 149 | Ar(4s ³ P ₁) + e → Ar(¹ P ₁) + e | 2.35 × 10 ⁻⁷ | [70] |
| 150 | Ar(4s ³ P ₁) + e → Ar(4s ³ P ₀) + e | 2.35 × 10 ⁻⁷ | [70] |
| 151 | Ar(4s ³ P ₁) + e → Ar ⁺ + e | <i>f</i> (<i>E</i> / <i>N</i>) | |
| 152 | Ar(4s ³ P ₁) + Ar(³ P ₀) → Ar ⁺ ₂ + e | 2.1 × 10 ⁻⁹ | [70] |
| 153 | Ar(4s ³ P ₁) + 2Ar → Ar ₂ ⁺ + Ar | 1.2 × 10 ⁻³² | [70] |
| 154 | Ar(4s ³ P ₁) → hv + Ar | 1 × 10 ⁸ | [59] |
| 155 | Ar(4s ³ P ₁) + O(³ P) → O(3p ³ P) + Ar | 1.38 × 10 ⁻¹¹ × (<i>T</i>) ^{1/2} | [72] |
| 156 | Ar(4s ³ P ₁) + O ₂ → Ar(¹ S) + O(¹ D) + O(¹ S) | 2.5 × 10 ⁻¹⁰ | [71] |
| 157 | Ar(4s ³ P ₁) + O ₂ (a ¹ Δ) → Ar(¹ S) + O ₂ ⁺ | 2.9 × 10 ⁻¹⁴ | [73] |
| 158 | Ar + e → Ar(4s ³ P ₀) + e | <i>f</i> (<i>E</i> / <i>N</i>) | |
| 159 | Ar(4p ³ P ₁) → hv + Ar(4s ³ P ₀) | 12.5 × 10 ⁶ | [59] |
| 160 | Ar(4p ¹ P ₁) → hv + Ar(4s ³ P ₀) | 19 × 10 ⁶ | [59] |
| 161 | Ar(4p ³ D ₁) → hv + Ar(4s ³ P ₀) | 2.6 × 10 ⁶ | [59] |
| 162 | Ar(4p ³ S ₁) → hv + Ar(4s ³ P ₀) | 0.9 × 10 ⁶ | [59] |
| 163 | Ar(4s ¹ P ₁) + e → Ar(4s ³ P ₀) + e | 3.1 × 10 ⁻⁷ | [70] |
| 164 | Ar(4s ³ P ₀) + e → Ar(4p ³ P ₁) + e | <i>f</i> (<i>E</i> / <i>N</i>) | |
| 165 | Ar(4s ³ P ₀) + e → Ar(4p ¹ P ₁) + e | <i>f</i> (<i>E</i> / <i>N</i>) | |
| 166 | Ar(4s ³ P ₀) + e → Ar(4p ³ D ₁) + e | <i>f</i> (<i>E</i> / <i>N</i>) | |
| 167 | Ar(4s ³ P ₀) + e → Ar(4p ³ S ₁) + e | <i>f</i> (<i>E</i> / <i>N</i>) | |
| 168 | Ar(4s ³ P ₀) + e → Ar(4p 4s ¹ P ₁) + e | 2.35 × 10 ⁻⁷ | [70] |
| 169 | Ar(4s ³ P ₀) + e → Ar ⁺ + e | <i>f</i> (<i>E</i> / <i>N</i>) | |
| 170 | Ar(4s ³ P ₀) + Ar(4s ³ P ₀) → Ar ⁺ ₂ + e | 1.2 × 10 ⁻⁹ | [70] |
| 171 | Ar(4s ³ P ₀) + Ar(4s ¹ P ₁) → Ar ⁺ ₂ + e | 2.1 × 10 ⁻⁹ | [70] |
| 172 | Ar(4s ³ P ₀) + 2Ar → Ar ₂ ⁺ + Ar | 11 × 10 ⁻³² | [70] |

Table 1 continued

| No | Process | Rate constants (s^{-1}) ($cm^3 s^{-1}$) ($cm^6 s^{-1}$) | Ref |
|-----|------------------------------------------------------------|--------------------------------------------------------------------|------|
| 173 | $Ar(4s^3P_0) + O(^3P) \rightarrow O(3p^3P) + Ar$ | $1.38 \times 10^{-11} \times (T)^{1/2}$ | [72] |
| 174 | $Ar(4s^3P_0) + O_2 \rightarrow Ar(^1S) + O(^1D) + O(^1S)$ | 2.4×10^{-10} | [71] |
| 175 | $Ar(4s^3P_0) + Ar \rightarrow Ar + Ar$ | 5.7×10^{-15} | [71] |
| 176 | $Ar + e \rightarrow Ar(4s^1P_1) + e$ | $f(E/N)$ | |
| 177 | $Ar(4p^1S_0) \rightarrow hv + Ar(4s^1P_1)$ | 45×10^6 | [59] |
| 178 | $Ar(4p^3P_1) \rightarrow hv + Ar(4s^1P_1)$ | 17×10^6 | [59] |
| 179 | $Ar(4p^3P_2) \rightarrow hv + Ar(4s^1P_1)$ | 23×10^6 | [59] |
| 180 | $Ar(4p^1P_1) \rightarrow hv + Ar(4s^1P_1)$ | 13×10^6 | [59] |
| 181 | $Ar(4p^1D_2) \rightarrow hv + Ar(4s^1P_1)$ | 5.3×10^6 | [59] |
| 182 | $Ar(4p^3D_1) \rightarrow hv + Ar(4s^1P_1)$ | 1×10^6 | [59] |
| 183 | $Ar(4p^3D_2) \rightarrow hv + Ar(4s^1P_1)$ | 1.4×10^6 | [59] |
| 184 | $Ar(4p^3S_1) \rightarrow hv + Ar(4s^1P_1)$ | 0.19×10^6 | [59] |
| 185 | $Ar(4s^1P_1) + e \rightarrow Ar(4p^1S_0) + e$ | $f(E/N)$ | |
| 186 | $Ar(4s^1P_1) + e \rightarrow Ar(4p^3P_1) + e$ | $f(E/N)$ | |
| 187 | $Ar(4s^1P_1) + e \rightarrow Ar(4p^3P_2) + e$ | $f(E/N)$ | |
| 188 | $Ar(4s^1P_1) + e \rightarrow Ar(4p^1P_1) + e$ | $f(E/N)$ | |
| 189 | $Ar(4s^1P_1) + e \rightarrow Ar(4p^1D_2) + e$ | $f(E/N)$ | |
| 190 | $Ar(4s^1P_1) + e \rightarrow Ar(4p^3D_1) + e$ | $f(E/N)$ | |
| 191 | $Ar(4s^1P_1) + e \rightarrow Ar(4p^3D_2) + e$ | $f(E/N)$ | |
| 192 | $Ar(4s^1P_1) + e \rightarrow Ar(4p^3S_1) + e$ | $f(E/N)$ | |
| 193 | $Ar(4s^1P_1) + e \rightarrow Ar^+ + e$ | $f(E/N)$ | |
| 194 | $Ar(4s^1P_1) + 2Ar \rightarrow Ar_2^+ + Ar$ | 1.2×10^{-32} | [70] |
| 195 | $Ar(4s^1P_1) \rightarrow hv + Ar$ | 5×10^8 | [59] |
| 196 | $Ar(4s^1P_1) + O(^3P) \rightarrow O(3p^3P) + Ar$ | $1.38 \times 10^{-11} \times (T)^{1/2}$ | [72] |
| 197 | $Ar(4s^1P_1) + O_2 \rightarrow Ar(^1S) + O(^1D) + O(^1S)$ | 3.1×10^{-10} | [71] |
| 198 | $Ar(4s^1P_1) + O_2(a^1\Delta) \rightarrow Ar(^1S) + O_2^+$ | 2.9×10^{-14} | [74] |
| 199 | $Ar + e \rightarrow Ar(4p^3S_1) + e$ | $f(E/N)$ | |
| 200 | $Ar + e \rightarrow Ar(4p^3D_3) + e$ | $f(E/N)$ | |
| 201 | $Ar + e \rightarrow Ar(4p^3D_2) + e$ | $f(E/N)$ | |
| 202 | $Ar + e \rightarrow Ar(4p^3D_1) + e$ | $f(E/N)$ | |
| 203 | $Ar + e \rightarrow Ar(4p^1D_2) + e$ | $f(E/N)$ | |
| 204 | $Ar + e \rightarrow Ar(4p^3S_1) + e$ | $f(E/N)$ | |
| 205 | $Ar + e \rightarrow Ar(4p^1P_1) + e$ | $f(E/N)$ | |
| 206 | $Ar + e \rightarrow Ar(4p^3P_2) + e$ | $f(E/N)$ | |
| 207 | $Ar + e \rightarrow Ar(4p^3P_1) + e$ | $f(E/N)$ | |
| 208 | $Ar + e \rightarrow Ar(4p^1S_0) + e$ | $f(E/N)$ | |
| 209 | $O(^3P) + e \rightarrow O(3s^3S) + e$ | $f(E/N)$ | |
| 210 | $O(3p^3P) + O_2(X) \rightarrow O(^1S) + 2O(^3P)$ | $4.62 \times 10^{-11} \times (T)^{1/2}$ | [69] |
| 211 | $O(3s^3S) + O_2(X) \rightarrow O(^1S) + 2O(^3P)$ | $9.81 \times 10^{-12} \times (T)^{1/2}$ | [69] |
| 212 | $O(3s^3S) + e \rightarrow O(3p^3P) + e$ | $f(E/N)$ | |
| 213 | $O(3p^3P) \rightarrow O(3s^3S) + hv$ | 2.8×10^7 | [75] |
| 214 | $O(3s^3S) \rightarrow O(^3P) + hv$ | 6.0×10^8 | [75] |
| 215 | $O(^3P) + e \rightarrow O(3p^3P) + e$ | $f(E/N)$ | |

Table 1 continued

| No | Process | Rate constants (s^{-1}) ($cm^3 s^{-1}$) ($cm^6 s^{-1}$) | Ref |
|-----|------------------------------------------------------|------------------------------------------------------------------|----------|
| 216 | $O_2(X) + e \rightarrow O(3p^3P) + O(^3P) + e$ | $f(E/N)$ | |
| 217 | $O_2(b) + Ar \rightarrow O_2(X) + Ar$ | 2.5×10^{-15} | [52] |
| 218 | $O_2(X) + e \rightarrow O(3s^3S) + O(^3P) + e$ | $f(E/N)$ | |
| 219 | $N_2O + e \rightarrow N_2(X) + O^-$ | $f(E/N)$ | |
| 220 | $O_2^- + N_2(X) \rightarrow O_2(X) + N_2(X) + e$ | $1.9 \times 10^{-12} \times (T/300)^{0.5} \times \exp(-4990/T)$ | [19, 26] |
| 221 | $NO_2 + e \rightarrow NO + O^-$ | $f(E/N)$ | |
| 222 | $O(^3P) + O_2(X) + e \rightarrow O^- + O_2(X)$ | 1×10^{-31} | [76, 77] |
| 223 | $O(^3P) + O_2(X) + e \rightarrow O(^3P) + O_2^-$ | 1×10^{-31} | [26] |
| 224 | $N(^4S) + NO_2 \rightarrow N_2(X) + O_2(X)$ | 7×10^{-13} | [52] |
| 225 | $N(^4S) + NO_2 \rightarrow N_2(X) + O(^3P) + O(^3P)$ | 9.1×10^{-13} | [52] |
| 226 | $N(^4S) + NO_2 \rightarrow N_2O + O(^3P)$ | 3×10^{-12} | [52] |
| 227 | $N(^4S) + NO_2 \rightarrow NO + NO$ | 2.3×10^{-12} | [52] |
| 228 | $O(^3P) + NO_2 \rightarrow NO + O_2(X)$ | $1.13 \times 10^{-11} \times (T/1,000)^{0.18}$ | [52] |
| 229 | $O(^3P) + NO_3 \rightarrow O_2(X) + NO_2$ | 1×10^{-11} | [52] |
| 230 | $O_2(X) + N_2(X) + e \rightarrow O_2^- + N_2(X)$ | $1.07 \times 10^{-31} \times (300/T_e) \times \exp(-70/T)$ | [35] |
| 231 | $NO + NO_3 \rightarrow NO_2 + NO_2$ | $1.79 \times 10^{-11} \times \exp(110/T)$ | [52] |
| 232 | $NO_2 + O_3 \rightarrow O_2(X) + NO_3$ | $1.2 \times 10^{-13} \times \exp(-2,450/T)$ | [52] |
| 233 | $NO_3 + NO_3 \rightarrow O_2 + NO_2 + NO_2$ | $5 \times 10^{-12} \times \exp(-3,000/T)$ | [52] |
| 234 | $NO_2 + NO_3 \rightarrow NO + NO_2 + O_2(X)$ | $2.3 \times 10^{-13} \times \exp(-1,600/T)$ | [52] |
| 235 | $O_2^- + O_2(X) \rightarrow O_2(X) + O_2(X) + e$ | $2.7 \times 10^{-10} \times (T/300)^{0.5} \times \exp(-5,590/T)$ | [26] |
| 236 | $N(^2P) + N(^2D) \rightarrow N_2^+ + e$ | 1×10^{-11} | [52] |
| 237 | $N_2(A) + O_2(X) \rightarrow N_2O + O(^3P)$ | 7.8×10^{-14} | [53] |
| 238 | $O(^1D) + N_2O \rightarrow NO + NO$ | 7.2×10^{-11} | [67] |
| 239 | $O(^1D) + N_2O \rightarrow N_2(X) + O_2(X)$ | 4.4×10^{-11} | [67] |
| 240 | $O_3 + e \rightarrow O^- + O_2$ | 1×10^{-11} | [78] |
| 241 | $O^- + O_2(X) \rightarrow O_3 + e$ | 5×10^{-15} | [76, 77] |
| 242 | $N(^4S) + O_2(X) \rightarrow NO(X) + O(^3P)$ | $1.1 \times 10^{-14} \times \exp(-3,150/T)$ | [52] |
| 243 | $H_2O + e \rightarrow H(^1S) + OH + e$ | $f(E/N)$ | |
| 244 | $OH + OH \rightarrow H_2O_2$ | $1.5 \times 10^{-11} \times T^{-0.4}$ | [79] |
| 245 | $OH + OH + O_2(X) \rightarrow H_2O_2 + O_2(X)$ | $6.5 \times 10^{-31} \times (300/T)^{-0.7}$ | [80] |
| 246 | $OH + OH + H_2O \rightarrow H_2O_2 + H_2O$ | $1.5 \times 10^{-31} \times (1/T)^2 \times \exp(22/T)$ | [27] |
| 247 | $OH + OH \rightarrow H_2O + O(^3P)$ | $2.9 \times 10^{-20} \times T^{2.6} \times \exp(945/T)$ | [81] |
| 248 | $OH + O_3 \rightarrow HO_2 + O_2(X)$ | $1.9 \times 10^{-12} \times \exp(-1,000/T)$ | [80] |
| 249 | $OH + H(^1S) + O_2(X) \rightarrow H_2O + O_2(X)$ | $6.9 \times 10^{-31} \times T^{-2}$ | [27] |
| 250 | $OH + H(^1S) + H_2O \rightarrow H_2O + H_2O$ | $4.4 \times 10^{-31} \times T^{-2}$ | [27] |
| 251 | $OH + H(^1S) \rightarrow H_2O$ | 2.7×10^{-14} | [82] |
| 252 | $OH + H(^1S) \rightarrow H_2(X) + O(^3P)$ | $1.38 \times 10^{-14} \times T \times \exp(-3,500/T)$ | [81] |
| 253 | $OH + O(^3P) \rightarrow O_2(X) + H(^1S)$ | $2.01 \times 10^{-11} \exp(112/T)$ | [81] |
| 254 | $OH + H_2 \rightarrow H_2O + H(^1S)$ | $7.69 \times 10^{-12} \times \exp(-2,000/T)$ | [81] |
| 255 | $OH + HO_2 \rightarrow H_2O + O_2(X)$ | $4.8 \times 10^{-11} \times \exp(250/T)$ | [81] |

Table 1 continued

| No | Process | Rate constants (s^{-1}) ($cm^3 s^{-1}$) ($cm^6 s^{-1}$) | Ref |
|-----|-------------------------------------------------------------------|--------------------------------------------------------------------|------|
| 256 | $O\dot{H} + H_2O_2 \rightarrow H_2O + HO_2\dot{}$ | $2.91 \times 10^{-12} \times \exp(-160/T)$ | [81] |
| 257 | $H(^1S) + H + M \rightarrow H_2(X) + M$ | $2.7 \times 10^{-31} \times T^{-0.6}$ | [81] |
| 258 | $H(^1S) + H_2O \rightarrow O\dot{H} + H_2(X)$ | $7.6 \times 10^{-16} \times T^{1.6} \times \exp(-9,281/T)$ | [81] |
| 259 | $H(^1S) + HO_2\dot{ } \rightarrow H_2(X) + O_2(X)$ | $7.11 \times 10^{-11} \times \exp(-710/T)$ | [81] |
| 260 | $H(^1S) + HO_2\dot{ } \rightarrow O\dot{H} + O\dot{H}$ | $2.81 \times 10^{-10} \times \exp(-440.2/T)$ | [81] |
| 261 | $H(^1S) + HO_2\dot{ } \rightarrow H_2O + O(^3P)$ | $5 \times 10^{-11} \times \exp(-866/T)$ | [81] |
| 262 | $H(^1S) + H_2O_2 \rightarrow H_2O + O\dot{H}$ | $1.69 \times 10^{-11} \times \exp(-1,780/T)$ | [81] |
| 263 | $H(^1S) + H_2O_2 \rightarrow HO_2\dot{ } + H_2(X)$ | $2.81 \times 10^{-12} \times \exp(-1,890/T)$ | [81] |
| 264 | $H(^1S) + O_3 \rightarrow O\dot{H} + O_2(X)$ | $1.1 \times 10^{-10} \times \exp(-480/T)$ | [80] |
| 265 | $H(^1S) + O_3 \rightarrow HO_2\dot{ } + O(^3P)$ | $1 \times 10^{-10} \times \exp(-480/T)$ | [80] |
| 266 | $H(^1S) + O_2(X) \rightarrow O + O\dot{H}$ | $3.7 \times 10^{-11} \times \exp(-8,450/T)$ | [80] |
| 267 | $H(^1S) + O_2(X) + O_2(X) \rightarrow HO_2\dot{ } + O_2(X)$ | $5.9 \times 10^{-32} \times (300/T)$ | [80] |
| 268 | $O(^3P) + O(^3P) + O_2(X) \rightarrow O_2(X) + O_2(X)$ | $1.3 \times 10^{-32} \times (300/T) \times \exp(-170/T)$ | [83] |
| 269 | $O(^3P) + O_2(X) + H_2O \rightarrow O_3 + H_2O$ | $9.9 \times 10^{-34} \times \exp(510/T)$ | [80] |
| 270 | $O(^3P) + O_2(X) + Ar \rightarrow O_3 + Ar$ | $8.99 \times 10^{-33} \times (T/298)^{-0.88} \times \exp(-442/T)$ | [84] |
| 271 | $O(^3P) + O_2(X) + O_2(X) \rightarrow O_3 + O_2(X)$ | $6.4 \times 10^{-35} \times \exp(663/T)$ | [83] |
| 272 | $O(^3P) + O_3 \rightarrow O_2(X) + O_2(X)$ | $1.8 \times 10^{-11} \times \exp(-2,300/T)$ | [83] |
| 273 | $O(^3P) + H_2(X) \rightarrow O\dot{H} + H(^1S)$ | $3.44 \times 10^{-31} \times (T/298)^{2.67} \times \exp(-3,162/T)$ | [81] |
| 274 | $O(^3P) + H_2O \rightarrow O\dot{H} + O\dot{H}$ | $1 \times 10^{-11} \times \exp(-550/T)$ | [80] |
| 275 | $O(^3P) + HO_2\dot{ } \rightarrow O\dot{H} + O_2(X)$ | $2.91 \times 10^{-11} \times \exp(200/T)$ | [81] |
| 276 | $O(^3P) + H_2O_2 \rightarrow O\dot{H} + HO_2\dot{ }$ | $1.4 \times 10^{-12} \times \exp(-2,000/T)$ | [81] |
| 277 | $O_3 + O_2(X) \rightarrow O(^3P) + O_2(X) + O_2(X)$ | $7.26 \times 10^{-10} \times \exp(-11,400/T)$ | [83] |
| 278 | $HO_2\dot{ } + O_3 \rightarrow O\dot{H} + O_2(X) + O_2(X)$ | $1.4 \times 10^{-14} \times \exp(-600/T)$ | [80] |
| 279 | $HO_2\dot{ } + H_2O \rightarrow H_2O_2 + O\dot{H}$ | $4.7 \times 10^{-11} \times \exp(-16,500/T) \times$ | [80] |
| 280 | $HO_2\dot{ } + HO_2\dot{ } \rightarrow H_2O_2 + O_2(X)$ | $2.2 \times 10^{-13} \times \exp(600/T)$ | [81] |
| 281 | $HO_2\dot{ } + HO_2\dot{ } + O_2(X) \rightarrow H_2O_2 + 2O_2(X)$ | $1.9 \times 10^{-33} \times \exp(-118/T)$ | [27] |
| 282 | $O_2(a) + H_2O \rightarrow O_2(X) + H_2O$ | 3×10^{-18} | [42] |
| 283 | $O_2(b) + H_2O \rightarrow O_2(X) + H_2O$ | 6.7×10^{-12} | [42] |
| 284 | $O(^1D) + H_2O \rightarrow OH + OH$ | 2.8×10^{-10} | [67] |
| 285 | $O(^1D) + H_2O \rightarrow H_2O + O(^3P)$ | 2.8×10^{-10} | [67] |
| 286 | $O(^1D) + H_2O \rightarrow H_2(X) + O_2(X)$ | 2.3×10^{-12} | [67] |
| 287 | $NO + O\dot{H} + O_2(X) \rightarrow HNO_2 + O_2(X)$ | $7 \times 10^{-31} \times (T/298)^{-2.6}$ | [85] |
| 288 | $NO + O\dot{H} + N_2(X) \rightarrow HNO_2 + O_2(X)$ | $7 \times 10^{-31} \times (T/298)^{-2.6}$ | [85] |
| 289 | $HNO_2 + O\dot{H} \rightarrow NO_2 + H_2O$ | $6.24 \times 10^{-12} \times (T/298) \times \exp(-68.5/T)$ | [86] |
| 290 | $NO + HO_2\dot{ } \rightarrow NO_2 + O\dot{H}$ | $3.4 \times 10^{-12} \times \exp(270/T)$ | [64] |
| 291 | $NO_2 + O\dot{H} + N_2(X) \rightarrow HNO_3 + N_2(x)$ | $1.6 \times 10^{-30} \times (T/298)^{-2.9}$ | [87] |
| 292 | $NO_2 + HO_2\dot{ } + N_2(X) \rightarrow HNO_3 + N_2 + O(^3P)$ | $1.8 \times 10^{-31} \times (T/298)^{-3.2}$ | [64] |
| 293 | $NO_2 + O\dot{H} \rightarrow NO + HO_2\dot{ }$ | $3.01 \times 10^{-11} \times \exp(-3,362/T)$ | [86] |
| 294 | $O(^1D) + NO_2 \rightarrow O_2(X) + NO$ | 3×10^{-10} | [88] |
| 295 | $NO_2 + H(^1S) \rightarrow NO + O\dot{H}$ | $4 \times 10^{-10} \times \exp(-341/T)$ | [89] |

Table 1 continued

| No | Process | Rate constants (s ⁻¹) (cm ³ s ⁻¹) (cm ⁶ s ⁻¹) | Ref |
|-----|---------------------------------------------------------------------------------------------------------|------------------------------------------------------------------------------------------------------------|----------|
| 296 | NO + H(¹ S) → HNO | 2.44 × 10 ⁻¹⁰ × (T/298) ^{-0.41} | [86] |
| 297 | NO + H(¹ S) + N ₂ (X) → HNO + N ₂ (X) | 1.34 × 10 ⁻³¹ × (T/298) ^{-1.32} × exp(-371/T) | [86] |
| 298 | NO + H(¹ S) + O ₂ (X) → HNO + O ₂ (X) | 1.34 × 10 ⁻³¹ × (T/298) ^{-1.32} × exp(-371/T) | [86] |
| 299 | NO + H(¹ S) + H ₂ O → HNO + H ₂ O(X) | 1.34 × 10 ⁻³¹ × (T/298) ^{-1.32} × exp(-371/T) | [86] |
| 300 | HNO + O(³ P) → OH + NO | 5.99 × 10 ⁻¹¹ | [86] |
| 301 | HNO + O(³ P) → H(¹ S) + NO ₂ | 4.63 × 10 ⁻¹⁸ | [86] |
| 302 | N(⁴ S) + O ₃ → NO + O ₂ (X) | 2 × 10 ⁻¹⁶ | [52] |
| 303 | N(⁴ S) + N(⁴ S) + M → N ₂ (A) + M | 8.27 × 10 ⁻³⁴ × exp(500/T) | [52] |
| 304 | O(³ P) + O(³ P) + N ₂ (X) → O ₂ (X) + N ₂ (X) | 2.76 × 10 ⁻³⁴ × exp(720/T) | [52] |
| 305 | O(³ P) + O ₂ (X) + N ₂ (X) → O ₃ + N ₂ (X) | 6.2 × 10 ⁻³⁴ × (300/T) ² | [52] |
| 306 | N ₂ (A) + N ₂ O → N ₂ (X) + N(⁴ S) + NO | 1 × 10 ⁻¹¹ | [90, 91] |
| 307 | N ₂ (A) + N ₂ (X) → N ₂ (X) + N ₂ (X) | 3 × 10 ⁻¹⁸ | [92] |
| 308 | O ₂ (a) + O ₃ → O ₂ (X) + O ₂ (X) + O(³ P) | 9.7 × 10 ⁻¹³ × exp(-1,564/T) | [93] |
| 309 | O(¹ D) + O ₃ → O ₂ (X) + O(³ P) + O(³ P) | 1.2 × 10 ⁻¹⁰ | [93] |
| 310 | NO + e → NO ⁺ + 2e | f(E/N) | |
| 311 | OH + HNO ₃ → H ₂ O + NO ₃ | 8.3 × 10 ⁻¹⁵ × exp(851/T) | [94] |
| 312 | N ₂ (X) + e → N ₂ ⁺ + 2e | f(E/N) | |
| 313 | O ₂ (X) + e → O ₂ ⁺ + 2e | f(E/N) | |
| 314 | H ₂ O ₂ → OH + OH | 3.0 × 10 ¹⁴ × exp(-24,430/T) | [79] |
| 315 | H ₂ O ₂ + O ₂ (X) → HO ₂ + HO ₂ | 9.0 × 10 ⁻⁸ × exp(-19,976/T) | [95] |
| 316 | O ₃ → O ₂ (X) + O(³ P) | 7.6 × 10 ⁻⁹ × exp(-12,270/T) | [96] |
| 317 | N ₂ (A) + N ₂ (X) → N ₂ (X) + N ₂ (X) | 1.5 × 10 ⁻¹⁶ | [90] |
| 318 | HNO ₃ + e → OH + NO ₂ ⁻ | 1.5 × 10 ⁻⁷ | [97] |
| 319 | Ar(4s ³ P ₂) + H ₂ O → Ar + OH(A,X) + H(¹ S) | 4.5 × 10 ⁻¹¹ | [98] |
| 320 | Ar(4s ³ P ₀) + H ₂ O → Ar + OH(A,X) + H(¹ S) | 4.5 × 10 ⁻¹¹ | [98] |
| 321 | Ar(4s ³ P ₁) + H ₂ O → Ar + OH(A,X) + H(¹ S) | 4.5 × 10 ⁻¹¹ | [98] |
| 322 | Ar(4s ¹ P ₁) + H ₂ O → Ar + OH(A,X) + H(¹ S) | 4.5 × 10 ⁻¹¹ | [98] |
| 323 | Ar + OH + H(¹ S) → Ar + H ₂ O | 2.59 × 10 ⁻³¹ × (T/298) ⁻² | [27, 79] |
| 324 | Ar(4s ³ P ₂) + H ₂ (X) → Ar + H(¹ S) + H(¹ S) | 3.9 × 10 ⁻¹¹ | [45] |
| 325 | Ar(4s ³ P ₀) + H ₂ (X) → Ar + H(¹ S) + H(¹ S) | 3.5 × 10 ⁻¹¹ | [45] |
| 326 | Ar(4s ³ P ₁) + H ₂ (X) → Ar + H(¹ S) + H(¹ S) | 9 × 10 ⁻¹¹ | [45] |
| 327 | Ar(4s ¹ P ₁) + H ₂ (X) → Ar + H(¹ S) + H(¹ S) | 1.1 × 10 ⁻¹⁰ | [54] |
| 328 | N ₂ (C) + H ₂ O → N ₂ (X) + H ₂ O | 3.9 × 10 ⁻¹⁰ | [84] |

f(E/N)—was calculated on EEDF. O₂(X), N₂(X), OH(X), NO(X), H₂O, Ar designate the ground electronic state. O₂(A), N₂(A), N₂(B), N₂(C), N₂(a) designate A³Σ_u⁺, A³Σ_v⁻, ³Π_g, ³Π_u, and a¹Σ_g⁺ states. T—gas temperature

* was calculated for every vibrational level of N₂

2. Using these values, the equations of vibrational kinetics were solved. The relative accuracy of calculation was 1 %. Vibrational level distributions were obtained.
3. The composition of plasma was found by solving the quasi-stationary equations of chemical kinetics of Table 1. The calculation relative accuracy for every concentration was 1 %.
4. Calculated concentrations and vibrational distributions were returned to point 1 and so on. The computational procedure was terminated when the particle concentrations change did not exceed the error limit of 1 %.

The lack of data on water molecules concentrations is the main problem for the modeling. For this reason, we used these values as fitting parameters to satisfy the measured emission intensities of some Ar lines.

Of course, this approach neglects heterogeneity of plasma since it uses the average parameters. The appropriate estimates carried out in study [24] confirm that the 0-D modeling describes well the order of concentration magnitude and their change at variation of discharge parameters.

Results and Discussion

Figure 3 shows the measured gas temperature at different pressures. The pressure increase results in a linear gas temperature growth from 1,040 to 1,455 K. At the same time the specific power [$J \times E = W$, J —current density (Fig. 3)] inputted to positive column is increased faster from 83 to 377 W/cm³. Approximately, such temperature dependence can be explained in the following way. Assuming constant values of W and heat conductivity coefficient, λ , the solution of heat conductivity equation gives the following expression for the temperature averaged on discharge cross-section, \bar{T} .

$$\bar{T} = T(R) + 0.125 \times (W/\lambda) \times R^2, \quad (1)$$

where R —discharge radius, $T(R)$ —temperature on the plasma–gas interface. The temperature growth from 1,040 up to 1,450 K results in the increase of λ by a factor of 1.28 [28]. R^2 is decreased by a factor of 2.5 (see Fig. 4, the increase in a discharge current density). Therefore, it can be expected that the increase in specific power leads to the increase in the temperature by a factor of $377/(83 \times 1.28 \times 2.5) = 1.42$. It gives the temperature of 1,477 K. This value is very close to the experimental one. In addition, it means that radiation losses of energy give a small input in a total energy balance of plasma. It is necessary to point out that the value of $1,750 \pm 150$ K was obtained for the same discharge at 30 mA in study [3] on the rotational structure of $A^2\Sigma \rightarrow X^2\Pi$ (0–0) band of OH radicals.

Using the measured temperature, we calculated the total concentration of particle ($P = N \times kT$) and values of reduced electric field strengths, E/N . The appropriate results are shown in Fig. 4. The shape of this dependence is typical for discharges burning in a diffusion mode.

The emission spectra of the discharge are represented in Figs. 5 and 6 for atmospheric pressure. At other pressures the spectrum view was qualitatively the same. The OES measurements showed the following lines and bands. Molecular nitrogen (N_2) was presented by slight bands of second positive system ($C^3\Pi_u \rightarrow B^3\Pi_g$). As it was mentioned above the (0–2) band was used for the temperature determination. Atomic oxygen was represented by two slight lines (777 and 845 nm; transition $3p^5P \rightarrow 3s^5S$ and

Fig. 3 The effective vibrational temperatures of molecules. $H_2O(100)$ —(1), $H_2O(001)$ —(2), —2, O_2 —(3), $H_2O(010)$ —(4). The gas temperature—(5)

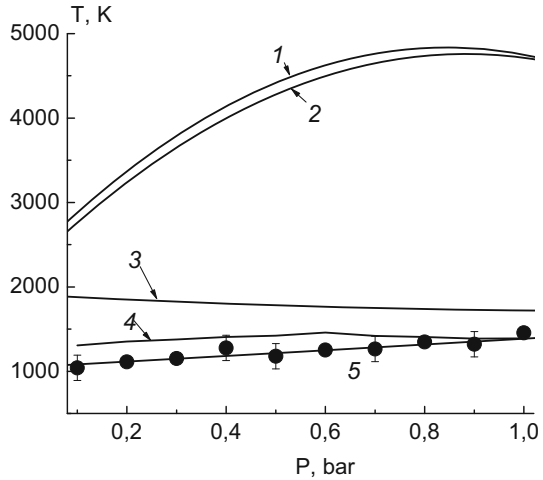
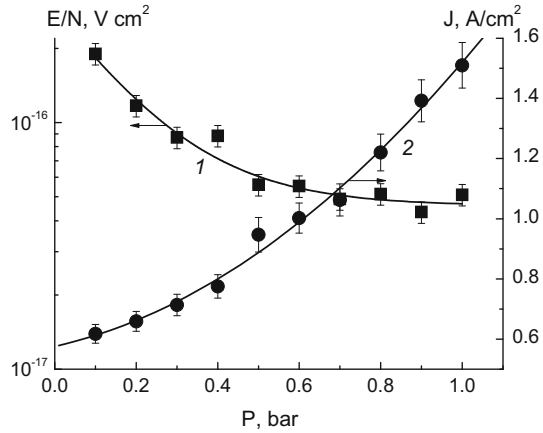


Fig. 4 The reduced electric field strength (1) and the discharge current density (2) on the half-height of positive column as a function of pressure



$3p^3P \rightarrow 3s^3S$, respectively). OH radicals exhibited two bands: $A^2\Sigma \rightarrow X^2\Pi$ (1–0, 0–0). Slight intensity bands of NO γ -system ($A^2\Sigma \rightarrow X^2\Pi$) were revealed as well. These intensities were essentially less than emission intensities of the argon lines. The irradiation of atomic hydrogen was represented by H_α (656) line. The emission lines of argon, which are listed in Table 2, were the most intensive.

These lines correspond to the transitions of the excited argon atoms in $4p^3S_1$, $4p^3D_1$, $4p^3D_2$, $4p^3D_3$, $4p^1D_2$, $4p^3P_0$, $4p^1P_1$, $4p^3P_2$, $4p^3P_1$, $4p^1S_0$ states to the lower metastable and resonance levels of Ar in $4s^3P_0$, $4s^3P_2$, $4s^3P_1$ and $4s^1P_1$ states. Among ten upper levels we used the transitions from seven ones since three $4p^3D_3$, $4p^3P_0$, $4p^1S_0$ levels give three lines (811.5, 751.5 and 750.4 nm respectively), which are either mutually overlapped ($4p^3P_0$ and $4p^1S_0$) or overlapped with another line ($4p^3D_3$ and $4p^3D_1$ at 810.4 nm). The real resolution of our optical system was 1.3 nm. The results of line intensities measurements are shown in Fig. 7.

Fig. 5 The discharge emission spectrum at atmospheric pressure for wave length range of 200–400 nm

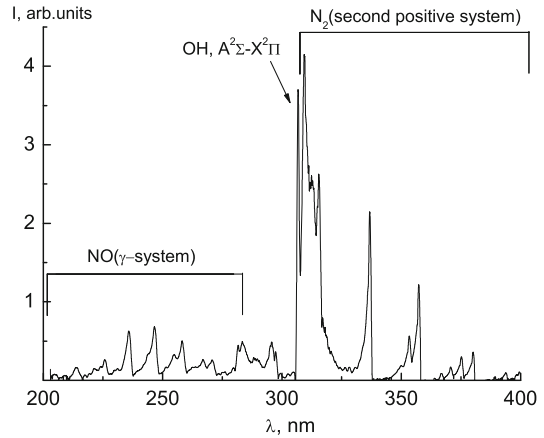
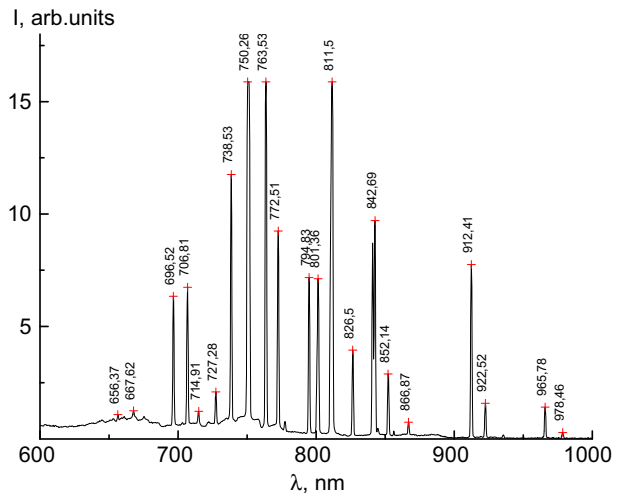


Fig. 6 The discharge emission spectrum at atmospheric pressure for wave length range of 600–1,000 nm



The calculations showed that the best agreement between the experimental intensities and the calculation (Fig. 7) is achieved at the water content represented in Fig. 8. The calculation shows that the water content at the pressure of 1 bar is 1.3 %. At the same time, the water content was estimated in study [3] as 8 % for 30 mA. The estimation was done on the base of the time evolution of LIF signal after the laser excitation was turned off. Authors assumed that the quenching of the upper level is exclusively due to the collisions with water molecules. Thus, to determine the water content, it is necessary to know the rate constant of this process at different temperatures. Unfortunately, authors do not give the constant value used, although they cite the study [29]. In this work, the calculation of cross-section was carried out at the room temperature only. Supposing that rate constant, k , can be written as

$$k = \sigma \times V,$$

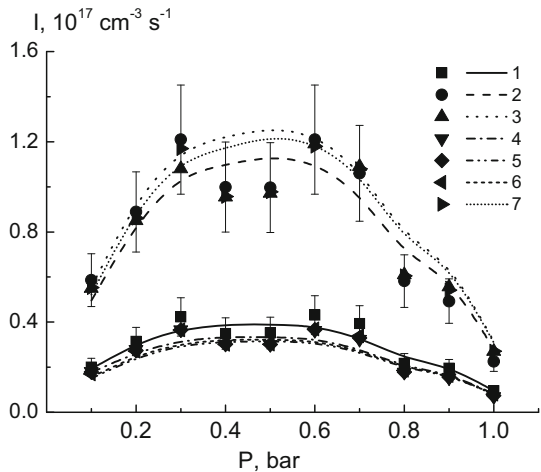
where σ —cross-section, $V = \sqrt{\frac{8kT}{\pi M}}$ —average velocity, for rate constant the following expression is obtained: $k = 1.47 \times 10^{-11} \times T^{0.5} \text{ cm}^3 \times \text{s}^{-1}$. At the temperature of

Table 2 The observed Ar emission lines

| N | Wave length (nm) | Transition | N | Wave length (nm) | Transition |
|----|--------------------|--------------------------------------------------------------------------------|----|--------------------|--------------------------------------------------------------------------------|
| 1 | 696.6 | Ar(4p ³ P ₁) → hv + Ar(4s ³ P ₂) | 11 | 811.5 | Ar(4p ³ D ₃) → hv + Ar(4s ³ P ₂) |
| 2 | 706.8 | Ar(4p ³ P ₂) → hv + Ar(4s ³ P ₂) | 12 | 826.5 ^a | Ar(4p ³ P ₁) → hv + Ar(4s ¹ P ₁) |
| 3 | 727.3 | Ar(4p ³ P ₁) → hv + Ar(4s ³ P ₁) | 13 | 840.8 | Ar(4p ³ P ₂) → hv + Ar(4s ¹ P ₁) |
| 4 | 738.4 ^a | Ar(4p ³ P ₂) → hv + Ar(4s ³ P ₁) | 14 | 842.5 ^a | Ar(4p ³ D ₂) → hv + Ar(4s ³ P ₁) |
| 5 | 750.4 | Ar(4p ¹ S ₀) → hv + Ar(4s ¹ P ₁) | 15 | 852.1 ^a | Ar(4p ¹ P ₁) → hv + Ar(4s ¹ P ₁) |
| 6 | 763.7 ^a | Ar(4p ¹ D ₂) → hv + Ar(4s ³ P ₂) | 16 | 866.8 | Ar(4p ³ D ₁) → hv + Ar(4s ³ P ₀) |
| 7 | 772.6 ^a | Ar(4p ³ D ₁) → hv + Ar(4s ³ P ₀) | 17 | 912.3 ^a | Ar(4p ³ S ₁) → hv + Ar(4s ³ P ₂) |
| 8 | 794.8 | Ar(4p ¹ P ₁) → hv + Ar(4s ³ P ₀) | 18 | 922.4 | Ar(4p ¹ D ₂) → hv + Ar(4s ¹ P ₁) |
| 9 | 801.5 | Ar(4p ³ D ₂) → hv + Ar(4s ³ P ₂) | 19 | 965.8 | Ar(4p ³ S ₁) → hv + Ar(4s ³ P ₁) |
| 10 | 794.8 | Ar(4p ³ D ₂) → hv + Ar(4s ³ P ₂) | 20 | 978.5 | Ar(4p ³ D ₂) → hv + Ar(4s ¹ P ₁) |

^a The lines intensities of which were chosen for measurement

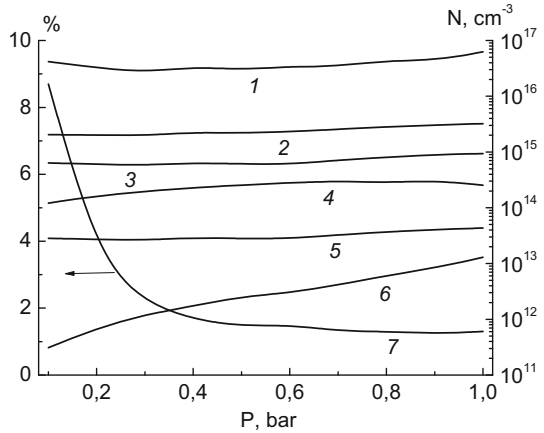
Fig. 7 The line intensities versus pressure. *Points*—experiment, *lines*—calculation. 1—Ar(4p³D₁) –772.6 nm; 2—Ar(4p³D₂) –842.5; 3—Ar(4p¹D₂) –763.7 nm; 4—Ar(4p¹P₁) –852.1 nm; 5—Ar(4p³P₂) –738.4 nm; 6—Ar(4p³P₁) 826.5 nm; 7—Ar(4p³S₁) 912.3 nm



1,750 K it gives the rate constant of $6.5 \times 10^{-10} \text{ cm}^3 \text{ s}^{-1}$. In study [3], the decay time was 30–50 ns. Therefore, water concentrations are $(5\text{--}3) \times 10^{16} \text{ cm}^{-3}$. At the temperature of 1,750 obtained in [3] and at the atmospheric pressure, the water content will be (0.7–1.2) %. These values are close to our data. It is interesting that in the next paper [30] authors used the correct value of the constant ($6.8 \times 10^{-10} \text{ cm}^3 \text{ s}^{-1}$).

Calculations showed that OH radical concentrations are slightly increased with a pressure growth, and it equals to $3.2 \times 10^{15} \text{ cm}^{-3}$ at the pressure of 1 bar (Fig. 8). The concentration of $2 \times 10^{14} \text{ cm}^{-3}$ was obtained in study [3] at the same conditions. We assume that such a low concentration is conditioned with the specific features of experimental set-up. Plasma-forming gas was inducted through above-water needle shape electrode having an orifice of 0.5 mm diameter. At a flow rate of 300 sccm it provides the gas flow velocity of $1.5 \times 10^4 \text{ cm s}^{-1}$. At the gap between the electrode and the water surface of 0.8 cm, it gives the residence time of $\sim 5 \times 10^{-5} \text{ s}$. Such short time means that gas flow

Fig. 8 The concentrations of H_2O (1), OH (2), H_2O_2 (3), $\text{O}(^3\text{P})$ (4), HO_2 (5), O_3 (6) molecules and H_2O mole fraction (7) versus pressure



rate can influence kinetics of some processes. In fact, our calculation showed that the main process of OH formation is reaction $\text{O}(^3\text{P}) + \text{H}_2\text{O} \rightarrow \text{OH} + \text{OH}$ (reaction N 271 of Table 1, rate is $1.1 \times 10^{20} \text{ cm}^{-3} \text{ s}^{-1}$) rather than $\text{H}_2\text{O} + \text{e} \rightarrow \text{OH} + \text{H}$ (reaction N 240 of Table 1, rate is $4.8 \times 10^{19} \text{ cm}^{-3} \text{ s}^{-1}$) as it is often assumed. The life time of $\text{O}(^3\text{P})$ in the reaction N 271 is $\sim 7 \times 10^{-4} \text{ s}$. Therefore, the gas flow has to affect strongly the concentration of $\text{O}(^3\text{P})$ leading to its decrease. As a result, OH concentration must drop. Some studies [3, 31] assume that the reactions with the lower excited states of Ar can play an important role in a water dissociation. However, the calculation shows that these reactions (N 316–319) are negligible in comparison with the reactions mentioned above (total rate is $1.2 \times 10^{17} \text{ cm}^{-3} \text{ s}^{-1}$) at least under the conditions of given discharge.

The gas pressure increase leads to the dropping E/N (Fig. 4). It results in the changes in EEDF, which are shown in Fig. 9. Such EEDF changes provide the decrease in the characteristic and average energies ($\bar{\epsilon}$) of electrons (Fig. 10) and their drift velocity. The latter leads to the growth of the electron density, N_e (Fig. 10). The average energy of electrons is 3.1 eV at an atmospheric pressure rather than 1 eV as it was estimated in study [3]. Due to the EEDF deformation the rate constants of electron impact are decreased with the pressure. The decrease rate depends on the process threshold energy. For the processes with low thresholds, the rate is less than for those with a higher threshold. As a result, the process rates can be increased, decreased or pass through maximum. It is clearly observed from a pressure course of line intensities (Fig. 7) and from the concentrations of lower states of Ar (Fig. 11). At the same time, the ionization rates for all species are decreased with pressure (Fig. 12).

The data obtained allow making suppositions on the ionization mechanism. The shape of E/N dependence on the pressure is typical for dischargers burning in a diffusion mode. In that mode, ionization rate is equal to charge losses on the plasma–gas interface. Charged particles reach the interface by means of their diffusion in a field of volume charge. And the total ionization frequency is equal to the diffusion frequency of charge losses. In the case of volume losses of charges in recombination processes the E/N dependence on pressure must be different. The increase in electron concentration and dropping electron average energy (increase in recombination rate constants) should result in the increase in the charge loss frequency. Therefore, for discharge supporting the higher ionization

Fig. 9 The electron energy distribution functions at different pressures. 1—0.1 bar, 2—0.5 bar and 3—1 bar

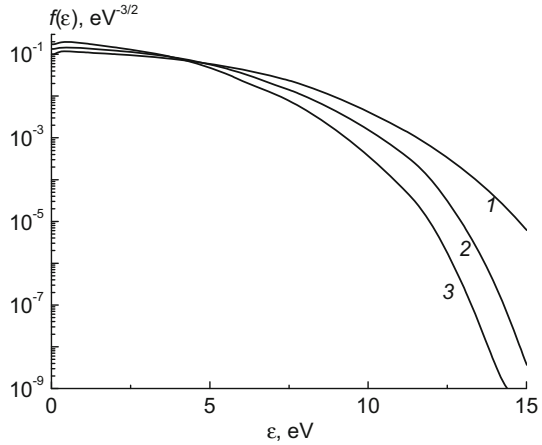
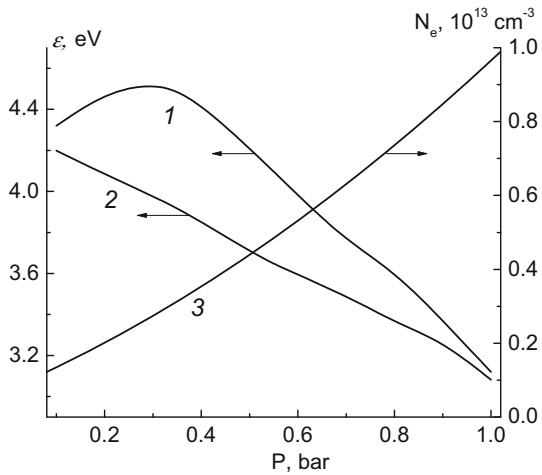


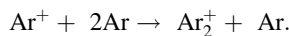
Fig. 10 The characteristic (1) and average (2) energies of electrons (1) and electron density (3) at different pressures



frequency is required. That is the E/N value must be increased with pressure. In the diffusion mode, the diffusion frequency, ν_D , equals to the ionization frequency, ν_i ,

$$\nu_D \approx (D_A \times 5.76)/R^2 = \nu_i, \tag{2}$$

where D_A is the coefficient of ambipolar diffusion. The ambipolar diffusion coefficient is determined as $D_A = \varepsilon_{ch} \times \mu^+$, where ε_{ch} is the electron characteristic energy and μ^+ is the positive ions mobility. The calculation of ionization frequencies (Fig. 12) showed that the Ar^+ ions must be primary ones. Further, Ar^+ primary ions should be fast converted into Ar_2^+ ions over the reaction



The reaction rate constant is $1.5 \times 10^{-31} \text{ sm}^6 \text{ s}^{-1}$ [32] so that the Ar^+ life time is less than $\sim 10^{-7} \text{ s}$. The Ar_2^+ ions mobility in Ar at standard conditions (273 K, 1 bar) is $1.8 \text{ cm}^2/(\text{V} \times \text{s})$ [33]. Taking into consideration that μ^+ depends on the total particle density as

Fig. 11 The concentrations of Ar($4s^3P_1$) (1), Ar($4s^3P_2$) (2), Ar($4s^3P_0$) (3) and Ar($4s^1P_1$) (4) states at different pressures

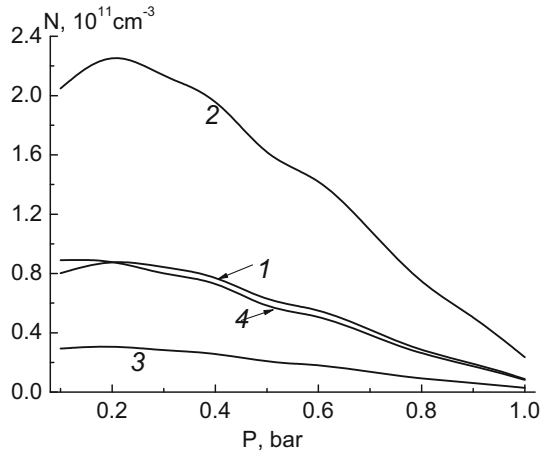
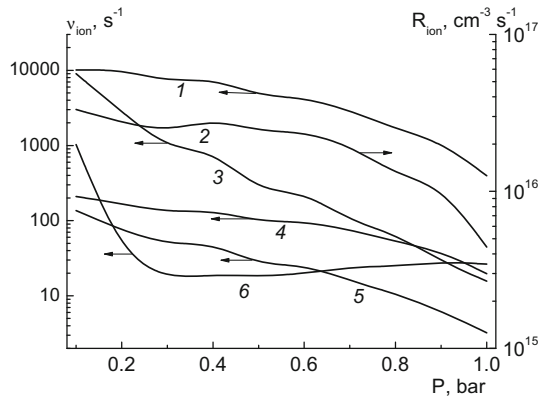


Fig. 12 Ionization frequencies. Stepwise ionization of Ar—(1), $H_2O(X)$ molecules—(3), $O_2(a^1\Delta_g)$ molecules (4), $O_2(X)$ —(5), direct ionization of Ar (6). The total ionization rate—(2)



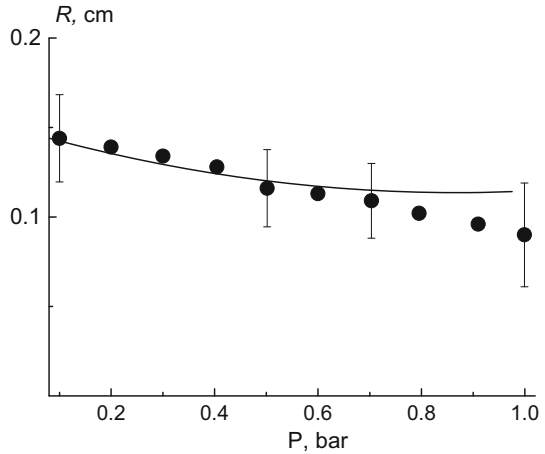
$1/N$ and on the temperature as $1/T$, we calculated the R value using ε_{ch} from Fig. 10. Comparing these data with the experimental ones (Fig. 13), we make the conclusion that the diffusion mode is more probable. In all range of pressure under study, the main primary process is the stepwise ionization of the four lowest excited states of Ar atom. For this reason, the reduced electric field strengths are essentially less than for the discharge in ambient air at the same pressure [2]. It necessary to point out that the authors of study [34] arrive at a conclusion on diffusion mode of discharge as well.

The data mentioned above allow creating the procedure for calculation of plasma properties using as input parameters only the discharge current density, total concentration of particles and water content. The output parameters would be the plasma composition, discharge current, positive column radius, gas temperature and pressure.

The iterative procedure can be the following.

1. The E/N , N , discharge current density, and gas temperature are specified. This is the first approximation.
2. Boltzmann equation and chemical kinetics equations are solved in a consecutive order.
3. Using equation of charges balance (2) the plasma radius is determined.

Fig. 13 The discharge radius, R , as a function of pressure. Points—experiment, line—calculation



4. The gas temperature is calculated on the heat conductivity Eq. (1).
5. Calculated temperature is returned to point 1 and so on.

After the convergence was achieved it is possible to determine the gas pressure ($P = N \times kT$) and the discharge current ($i = \pi R^2 \times J$). We plan to carry out such calculation hereafter.

The vibrational temperatures for H_2O and $\text{O}_2(\text{X})$ determined on the population of first two levels are represented in Fig. 3. Vibrational temperatures for $\text{O}_2(\text{X})$ and H_2O (010) mode are close to the gas ones. The slight dependence of vibrational temperatures on the pressure is related with slight dependence of excitation-de-excitation constants by electron impact for the first vibrational levels on the pressure due to low threshold energy of vibrational levels excitation. Unlike air plasma [21] it should be noted that the determination of vibrational distributions is not necessary in the case of argon plasma since vibrational excited molecules do not really influence both EEDF and processes in a gas phase.

Also, the results obtained revealed that it is necessary to take into consideration the emission reabsorption since it affects strongly the calculation results especially under atmospheric pressure. Thus, the concentration of lower excited states of Ar ($^3\text{P}_1, ^3\text{P}_2, ^3\text{P}_0, ^1\text{P}_1$) calculated with reabsorption at atmospheric pressure were 8.8×10^9 , 2.4×10^{10} , 2.9×10^9 and $8.5 \times 10^9 \text{ cm}^{-3}$, respectively, whereas without reabsorption they were 7.8×10^8 , 1.9×10^{10} , 1.8×10^9 and $2.9 \times 10^8 \text{ cm}^{-3}$, respectively.

Conclusion

In the present study, the DC discharge in Ar was examined in a pressure range of 0.1–1 bar at the discharge current of 40 mA. The changes in the gas temperatures, electric field strengths and intensities of some Ar lines were measured. On the base of these data, the model of discharge was developed. The model included the joint solution of Boltzmann equation, equations of vibrational kinetics and equations of chemical kinetics. Calculations on that model agree well with measured line intensities. The main species of plasma were H_2O , OH, H_2O_2 , $\text{O}(^3\text{P})$ and HO_2 . It was shown that the slow increase in a gas temperature

with pressure is due to the growth of inputted power and heat conductivity coefficient and the decrease in a radius of plasma. The ionization mechanism was analyzed. The data obtained indicate that discharge burns in diffusion mode, at which the stepwise ionization rate of the four lowest excited states of Ar is equal to the rate of charge diffusion loss.

Acknowledgments This study was supported by the RFBR Grant, Project No. 14-02-01113 A.

Reference

1. Bruggeman P, Leys C (2009) *J Phys D Appl Phys* 42(5):053001
2. Titov VA, Rybkin VV, Maximov AI, Choi H-S (2005) *Plasma Chem Plasma Process* 25(5):502–518
3. Li L, Nikiforov A, Xiong Q, Lu X, Taghizadeh L, Leys C (2012) *J Phys D Appl Phys* 45(12):125201
4. Nikiforov A, Li L, Xiong Q, Leys C, Lu XP (2011) *Eur Phys J Appl Phys* 56(2):23013–24009
5. Ito H, Kano H (2008) *Appl Phys Express* 1:10601–10603
6. Liu DX, Bruggeman P, Iza F, Rong MZ, Kong MC (2010) *Plasma Sources Sci Technol* 19(2):025018
7. Mirakami T, Niemi K, Gans T, O’Connell D, Graham WG (2013) *Plasma Sources Sci Technol* 22(1):01503
8. Van Gaens W, Bogaerts A (2013) *J Phys D Appl Phys* 46(27):275201
9. Shiqiang Zhang S, Van Gaens W, Van Gessel B, Hofman S, Van Veldhuizen E, Bogaerts A, Bruggeman P (2013) *J Phys D Appl Phys* 46(20):205202
10. Van Gaens W, Bruggeman PJ, Bogaerts A (2014) *New J Phys* 16: 063054
11. Gordiets B, Ferreira CM, Nahorny J, Pagnon D, Touzeau M, Vialle M (1996) *J Phys D Appl Phys* 29(4):1021–1031
12. Smirnov SA, Rybkin VV, Kholodkov IV, Titov VA (2002) *High Temp* 40(3):323–330
13. Puech V, Torchin L (1986) *J Phys D Appl Phys* 19(12):2304–2309
14. Gordiets BF, Ferreira CM, Guerra VL, Loureiro J, Nahorny J, Pagnon D, Touzeau Vialle M (1995) *IEEE Trans Plasma Sci* 23(23):750–768
15. Kajita S, Ushiroda S, Kondo Y (1990) *J Phys D Appl Phys* 67(9):4015–4023
16. Rybkin VV, Titov VA, Kholodkov IV (2008) *Izv Vyssh Uchebn Zaved Khim Khim Tekhnol* 51(3):3–10 (in Russian)
17. Rybkin VV, Titov VA, Kholodkov IV (2009) *Izv Vyssh Uchebn Zaved Khim Khim Tekhnol* 52(12):3–10 (in Russian)
18. Laher RR, Gilmore FR (1990) *J Phys Chem Ref Data* 19(1):277–304
19. Louriero J, Ferreira CM (1989) *J Phys D Appl Phys* 22(11):1680–1691
20. Diamy A-M, Legrand J-C, Smirnov SA, Rybkin VV (2005) *Contr Plasma Phys* 45(1):5–21
21. Titov VA, Rybkin VV, Smirnov SA, Kulentsan AN, Choi H-S (2006) *Plasma Chem Plasma Process* 26(6):543–555
22. *Physical-Chemical Processes in a Gas Dynamics. V. 1. Dynamics of physical–chemical processes in gas and plasma* (1995) Ed. Chernyy GG and Losev SA. Moscow, MSU (in Russian)
23. Lide DR (2003–2004) *Handbook of chemistry and physics*. CRC Press, New York
24. Bobkova ES, Smirnov SA, Zalipaeva YuV, Rybkin VV (2014) *Plasma Chem Plasma Process* 34(4):721–743
25. Alexandrov NL (1988) *Adv Phys Sci (Uspekhi Fizicheskikh Nauk)* 154 (2): 177–206 (in Russian)
26. Eliasson B, Kogelschatz U (1986) *Basic data for modeling of electrical discharges in gases: oxygen*. Brown Boveri Research Report KLR86-11C
27. Fehsenfeld FC, Albritton DL, Burt JA (1969) *Can J Chem* 47(10):1793–1795
28. Phelps AV (1969) *Can J Chem* 47(10):1783–1793
29. Kenner RD, Ogryzlo EA (1980) *Intern J Chem Kinet* 12(7):502–508
30. Fehsenfeld FC, Ferguson EE, Schmeltekopf AL (1966) *J Chem Phys* 45(5):1844–1845
31. Slinger TG, Black G (1979) *J Chem Phys* 70(7):3434–3443
32. Dvoryankin AN, Ibragimov LB, Kulagin YA, Shelepin LA (1987) *Mechanisms of electron relaxation in atomic-molecular media*. In: Smirnov BM (ed) *Plasma Chemistry*. Moscow, Energoatomizdat (in Russian)
33. Zinn J, Sutherland CD, Stone SN, Dunkan LM (1982) *J Atmos Terr Phys* 44(12):1143–1171
34. Young RA, Black G (1967) *J Chem Phys* 47(7):2311–2318
35. Smirnov BM (1982) *Excited atoms*. Moscow, Energoizdat (in Russian)
36. Slinger TG, Black G (1981) *J Chem Phys* 75(5):2247–2251

37. Slanger TG, Black G (1976) *J Chem Phys* 64(9):3763–3766
38. Atkinson R, Welge KH (1972) *J Chem Phys* 57(9):3689–3693
39. Kossyi IA, Kostinskiy IA, Matveev AA, Silakov VP (1994) Plasma chemical processes in non-equilibrium nitrogen-oxygen mixture. *Proc Inst Gen Phys RAS* 47:37–57 (in Russian)
40. Alexandrov NL (1978) *Tech Phys (Zhurnal Tekhnicheskoi Fiziki)* 48(7):1428–1431 (in Russian)
41. Kozlov SI, Vlaskov VA, Smirnova NV (1988) *Space Res* 26(5):738–745 (in Russian)
42. Smith K (1981) Tomson R Numer model gas lasers. Mir, Moscow (in Russian)
43. Krivonosova OE, Losev SA, Nalivaiyko VP (1987) Advisable data on rate constants of chemical reactions between molecules consisting from N and O atoms. In: Smirnov BM (ed) *Plasma chemistry. Energoatomizdat, Moscow* (in Russian)
44. Jannuzzi MP, Jeffries JB, Kaufman F (1982) *Chem Phys Lett* 87(6):570–574
45. Piper LG, Caledonia GE, Kennelaly JP (1981) *J Chem Phys* 75(6):2847–2853
46. Silakov VP (1990) Mechanism of supporting the long-lived plasma in molecular nitrogen at high pressure. Preprint of Moscow Engineering Physical Institute N 010–90M (in Russian)
47. Slovetkiy DI (1980) Mechanisms of chemical reactions in non-equilibrium plasma. Moscow, Mir (in Russian)
48. Piper LG (1982) *J Chem Phys* 77(5):2373–2377
49. Young RA, Black G, Slanger TG (1970) *J Chem Phys* 51(1):116–121
50. Radtsig AA, Smirnov BM (1980) Handbook on atomic and molecular physics. Atomizdat, Moscow (in Russian)
51. Piper LG (1987) *J Chem Phys* 87(3):1625–1629
52. Yaron M, Von Engel A, Vidaud PH (1976) *Chem Phys Lett* 37(1):159–161
53. Didyukov AI, YuA Kulagin, Shelepin LA, Yarygina VN (1989) *Quantum Electron* 16(5):892–904 (in Russian)
54. O'Brien RJ, Myers GH (1970) *J Chem Phys* 53(10):3832–3835
55. Yau AW, Shepherd GG (1979) *Planet Space Sci* 27(4):481–490
56. Husain D, Mitra SK, Young AN (1974) *J Chem Soc Faraday Trans Part II* 70(10):1721–1731
57. Delcroix JL, Ferreira CV, Ricard F (1973) Proceedings of the XI International Conference Phenomena in Ionized Gases: invited papers. Prague. 301
58. Baulch DL, Cox RA, Crutzen PJ (1982) *J Phys Chem Ref Data* 11(2):327–496
59. Bukharin EB, Lobanov AN (1984) Proc IV All-USSR symp plasma chem, Dnepropetrovsk, pp 52–53 (in Russian)
60. Dmitrieva IK, Zenevich VA (1984) *Russ J Phys Chem B Focus Phys (Zhurnal Khimicheskoi Fiziki)* 3(8):1075–1080 (in Russian)
61. Ivanov VV, Klopovskii KS, Lopaev DV, Rakhimov AT, Rakhimova TV (2000) *Plasma Phys Rep* 26(11):980–990
62. Karoulina EV, YuA Lebedev (1992) *J Phys D Appl Phys* 25(3):401–412
63. Smirnov BM (1974) Ions and excited atoms. Moscow, Atomizdat (in Russian)
64. Karasheva NN, Otorbaev DK, Ochkin VN (1985) *Proc Phys Ins USSR Acad Sci* 157:177 (in Russian)
65. Clark JD, Masson AJ, Wayne RP (1972) *Mol Phys* 23(5):995–1005
66. Morozov II, Temchin CM (1990) Reactions kinetics of singlet oxygen in a gas phase. In: Smirnov BM (ed) *Plasma Chemistry Atomizdat, Moscow* (in Russian)
67. Moore CE (1976) Selected tables of atomic spectra, atomic energy levels and multiplet tables-OI. National Bureau of Standards US Section 7, pp 1–30
68. Bastien F, Haug R, Lecuiller M (1975) *J Chim Phys* 72(1):105–112
69. Pace L (1978) *IEEE J Quant Electron* 14(4):263–274
70. Smirnov BM (1978) Negative ions. Moscow, Atomizdat (in Russian)
71. Baulch DL, Cobos CJ, Cox RA, Esser C, Franec P, Just Th, Kerr JA, Pilling MJ, Troe J, Walker RN, Warnatz J (1992) *J Phys Chem Ref Data* 21(3):411–429
72. Peyrous R, Rigolet P, Held BJ (1989) *J Appl Phys D Appl Phys* 22(11):1658–1667
73. Chirokov A Self-organization of microdischarges in DBD plasma. Master Thesis Drexel University
74. Tschikubo F, Ushida S, Watanabe T (2004) *Jpn J Appl Phys* 43(1):315–320
75. Smedt FD, Bui XV, Nguyen TL, Peeters J, Vereecken L (2005) *J Phys Chem* 109(1):2401–2409
76. Pontiga F, Soria C, Casrellanos A, Skalny JD (2002) *Ozone Sci Eng* 24(6):447–462
77. DeMore WB, Sander SP, Golden DM, Hampson RF, Kurylo MJ, Howard CJ, Ravishankara AR, Kolb CE, Molina MJ (1997) Chemical kinetics and photochemical data for use in stratospheric modeling. Evaluation number 12. JPL Publication 97-4
78. Tsang W, Herron JT (1991) *J Phys Chem Ref Data* 20(4):609–663
79. Hipple H, Krasteva N, Nasterlack S, Striebel F (1999) *J Chem Phys A* 110(14):6781–6788
80. Gauthier MJE, Snelling DR (1975) *J Photochem* 4(1):27–50

81. Su M-C, Kumaran SS, Lim KP, Michael JV, Wagner AF, Hardling LB, Fang D-C (2002) *J Phys Chem A* 106(36):8261–8270
82. Young RA, Black G, Slanger TG (1969) *J Chem Phys* 50(1):303–308
83. Taylor GW, Setser DW (1971) *J Am Chem Soc* 93(19):4930–4932
84. Clark WG, Setser DW (1980) *J Phys Chem* 84(18):228–2233
85. Arnold J, Comes FJ (1980) *Chem Phys* 47(1):125–130
86. Smith CA, Molina LT, Lamb JJ, Molina MJ (1984) *Int J Chem Kinet* 16(1):41–55
87. Novicki S, Krenos J (1988) *J Chem Phys* 89:031–7032
88. Tsang W, Hampson RF (1986) *J Phys Chem Ref Data* 15(3):1087–1279
89. Benson SW, Axworthy AE (1957) *J Chem Phys* 26:1718–1726
90. Shuman NS, Miller TM, Viggiano AA (2012) *J Chem Phys* 136(12):124307
91. Pancheshnyi SV, Starikovskaia SM, Starikovskii AY (1998) *Chem Phys Lett* 294(6):523–527
92. Smirnov SA, Rybkin VV, Ivanov AN, Titov VA (2007) *High Temp* 45(3):291–297
93. Hanley HJM (1973) *J Phys Chem Ref Data* 2(3):619–642
94. Bailey AE, Heard DE, Henderson DA, Paul PH (1999) *Chem Phys Lett* 302(1–2):132–138
95. Li L, Nikiforov A, Xiong Q, Britun N, Snyders R., Lu X, Leys C (2013) *Phys Plasmas* 20(9): 093502
96. Verreycken T, Schram DC, Leys C, Bruggeman P (2010) *Plasma Sources Sci Technol* 19(4): 045004
97. McDaniel EW, Mason EA (1973) *The mobility and diffusion of ions in gases*. Wiley, New York
98. Staack D, Farouk B, Gutsol A, Fridman A (2005) *Plasma Sources Sci Technol* 14(4):700–711